IL NUOVO CIMENTO **43 C** (2020) 19
DOI 10.1393/ncc/i2020-20019-2

Colloquia: FATA 2019

The path to the "ideal" brain PET imager: The race is on, the role for TOF PET

Stanislaw Majewski
University of California Davis - Davis, CA, USA

received 2 March 2020

Summary. — With the efforts under way to improve spatial resolution of the revolutionary Explorer family of imagers, the acute need to develop dedicated imagers for breast, prostate, heart, etc. may slowly disappear, except for some specialized cases in treatment guidance and monitoring, for example in proton therapy. It is in fact happening already. Part of the reason is the high cost of the dedicated systems but also an intriguing emerging opportunity that long axial length PET scanners can be equipped with magnifying inserts that can locally boost the resolution, as per the so-called virtual pinhole concept by Yuan-Chuan Tai from WashU, also called Zoom-in PET. However, the exception are the brain imaging scanners. The special geometry of the optimal helmet type designs for imaging of the brain still gives the opportunity to the brain PET imager developers to compete for the "best" system. We all want to produce good quality dynamic molecular PET brain images at low injected radiation doses (and... low cost). Several designs are being proposed as well as being built at this time in many places around the world. These designs mostly fall in two categories: 1) the mini-Explorer cylindrical type or 2) the compact helmet type, both with large angular brain coverage assuring high sensitivity. Due to the compact sizes of the helmet-type systems, in order to substantially benefit from the improved TOF performance, one needs to achieve better than 100 ps FWHM timing performance. In fact, 50 ps FWHM would be a very nice goal. Several groups are working on such concepts. In this race, any new ideas from the expert instrumentation community (not only the medical one) are highly encouraged, as a great impact is expected on brain imaging once such high-performance but also dissemination-ready (*i.e.*, robust and economical) designs are developed. Ideally, the brain imagers of the next generation will have high sensitivity and high spatial resolution approaching the predicted physical limit (due to positron range plus non-collinearity of the two emitted annihilation photons), limited to about 1 mm FWHM. Interestingly, there is a known connection between spatial resolution and sensitivity in detecting small lesions or structures, through the Partial Volume Effect (PVE). The adversarial effect of poor resolution on the detection of small structures is the blurring of the signal with the background. Inversely, if there is not enough statistics (detected/recorded events) per reconstruction voxel, even the best spatial resolution will not bring the tomographic uptake signal above the noisy background.

1. – Introduction

This review/opinion paper is based on a many-year intellectual and investigational journey of the author who was witnessing, investigating and participating in the dramatic progress in the field of dedicated brain PET [1-8]. The information collection was not just based on a review of the published literature or materials presented at the conferences, but often involved direct interaction with the developers. What is important, the author himself was and still is actively involved in this activity and many of the colleagues contacted for information were in fact his competitors, or collaborators. The guiding principle for the author through all these years was not to have one pre-decided concept of the "best" brain imager and pursue it. An interesting twist is that the author was the developer of the unique wearable brain imager [9-13]. The concept was based on the ideas of developers before, like Seiichi Yamamato's PET-Hat [14, 15] and also followed by another group [16] so there was always a "danger" of just closing oneself in that one particular area and being the (biased) promoter of that approach. It did not happen, and actually the author admits changing ideas quite often (to the confusion of others) but at each turn it was logically based on the new acquired information, novel ideas, new results, new simulations, etc. For a scientist (with a PhD in experimental high-energy physics) this dynamic intellectual story is fascinating to take part in. The driver always was the strong conviction that better brain imagers will have important impact on brain health, with screening for dementia with truly early diagnosis enabling effective treatment at the top of the dreams. Many people contributed to the pool of information, due to space limitation only partially represented here, and their list is included in the acknowledgements.

2. – Dedicated brain scanners

2˙1. *Initial rationale.* – PET is an excellent proven modality in imaging cancer, dementia and many other brain diseases, as well as in neuroscience (study of the healthy brain as well as diseased brain) [17-29]. However, this nuclear medicine modality suffers from the stigma of radiation exposure to all organs of the human body as the injection of the radioactive imaging agent is systemic and the agent is distributed through the blood stream in the whole body, independently of the organ of interest and of the rationale for the prescribed scan, and all organs are exposed, while some organs are more sensitive to radiation than other organs.

This radiation exposure concerns seriously limit at present the application of this powerful molecular imaging modality for example in early detection (screening) and development of treatment for Alzheimer's disease, stroke or traumatic brain injury (TBI), but also in depression and drug addiction, or in pediatric patients. Introduction of high-sensitivity imagers can change this situation and enable application of PET to many other clinical protocols.

The broad need to develop dedicated PET brain imagers was driven by the fact that the standard whole-body PET scanners, even the best like Siemens Biograph Vision [30, 31] are not optimized for brain imaging (figs. 1, 2). Indeed, both sensitivity and spatial resolution are suboptimal for many of the brain imaging tasks. Most of the emitted brain radiation from uptake of imaging agents escapes undetected in the standard multi-ring PET scanners placed far away from the patient's head. In addition, standard PET scanners are not optimized for dynamic operation with kinetic analysis that offers new levels of diagnostic precision.

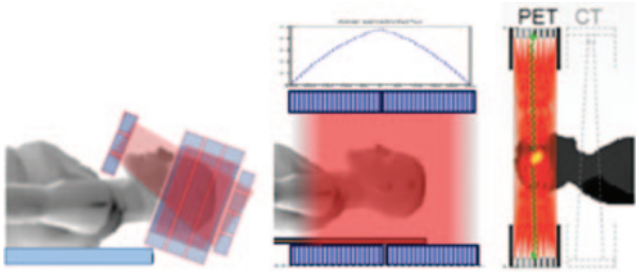

Fig. 1. – Two major geometries as options for a dedicated brain PET imager. On the right we show the standard brain imaging geometry of the clinical PET/CT scanner. On the left we show an example of a tight compact (but not wearable) helmet design. The TopHat compact helmet-style robust imager shown here, unlike other helmet designs, avoids curved surfaces at the top and bottom. Two detector panels, above and below the head, are added to the central multi-ring cylinder section. The mini-Explorer type approach is shown in the middle. This cylindrical design may have about 50 cm axial length, with improved 3D spatial resolution (smaller scintillator pixelation and good DOI), and with improved TOF timing compared to the total-body Explorer design.

Also, there are several clinical applications where having bedside, mobile, motion-tolerant PET brain imaging is highly advantageous compared to the standard PET imaging with the bulky and immobile, "bolted to the floor" clinical PET scanners typically in the form of the PET/CT tandems (fig. 3). These applications are in diagnostics and in treatment, surgery, radio-surgery, etc. When quick imaging is necessary and there is no time to transport the patient to the PET scanner, there is a need for a mobile scanner that can be "brought to the patient" in ER, ICU, surgery, trauma clinic, etc. One of the critical identified situations with acute need for such a quick imaging protocol is

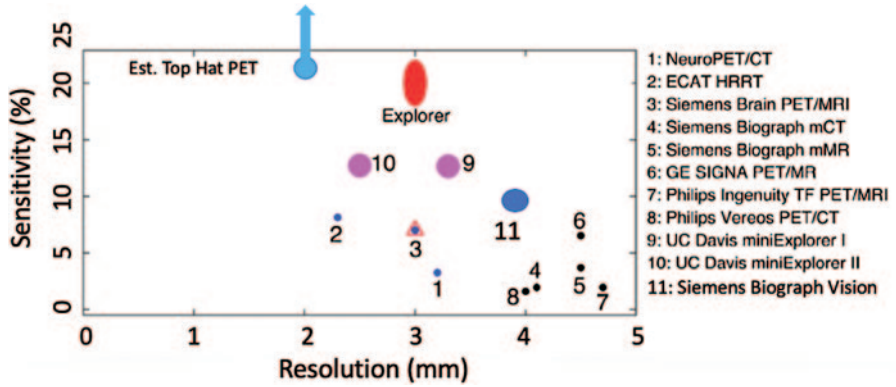

Fig. 2. – "World plot" of sensitivity (in the center of the scanner) *vs.* resolution in dedicated brain PET scanners plus uExplorer. Status from mid-2019 (modified by the author from the original plot by Junwei Du, UC Davis). The record of sensitivity is held at this point by uExplorer at ∼20%. The record of resolution below 2.5 mm still belongs to the Siemens HRRT scanner [32-35]. As an example, the sensitivity estimate for one of the novel helmet designs (Top Hat PET from fig. 1) puts it at 25% or higher. Spatial resolution is estimated at ∼2 mm FWHM or better.

Fig. 3. – Two practiced geometries in modern brain PET imaging. With the conventional PET scanner shown on the left the head is positioned in the center of and far from a large-diameter PET cylinder with the horizontal bore. The standard PET scanner is bulky and not mobile, typically used as a PET/CT tandem (shown in the picture is the mCT scanner from Siemens), and that requires patient transportation to the scanner typically located in the PET facility of the medical center. Precious time is lost before imaging can start. The dedicated brain scanners shown in the center (Helmet-Neck PET, Japan, see Yamaya *et al.* [36-38]) and at right (CareMIBrain mobile imager [6,7] from Oncovision, Valencia, Spain) provide increased 3D angular coverage and higher resolution. Both imagers are mobile and can be used at bedside, both have a rather tight tube detector design and are placed at fixed angles, while the challenge is how to perform quick and safe insertion of the patient's head.

imaging patients after TBI. The purpose of imaging is to identify and then subsequently assist in treatment (for example by guiding the surgery) of the brain site(s) involved in the trauma. The PET imaging scan needs to start promptly but also *needs to provide flexible positioning and be safe to the patient.*

Finally, some research brain imaging applications could also benefit from the availability of mobile, portable, upright and even "wearable" compact systems, as opposed to the conventional PET scanners with patients placed on scanning tables in the horizontal (supine or prone) positions.

The dedicated brain PET development trajectory over the last two decades was largely following the advances in the imaging technology. The first generation of dedicated brain imagers was based on the standard vacuum photomultiplier (PMT) + crystal scintillator (BGO) array technology but arranged in tighter rings surrounding the head of the patient. The second generation is using more compact position sensitive vacuum PMTs and the latest variants are based on the solid-state Silicon Photomultiplier (SiPM) technology. Especially the MRI capability of the latest generation of solid-state based photosensor technology (APDs and SiPMs) enabled designs of PET inserts in MRI scanners and many such systems were developed and new products are under development (example: MindView [8, 39, 40] from Oncovision).

The need for the new design stems from the fact that so far none of the developed PET imagers that can image human brain was designed to reach the limit in resolution while maintaining high sensitivity, that is *necessary to benefit from the high resolution*. With the conventional PET/CT scanner the head is positioned in the center of the field of view and far from a large-diameter PET ring. Dedicated PET brain scanners like CareMiBrain [6, 7] provide tighter geometry close to the head and increased 3D angular coverage resulting in higher sensitivity compared to conventional scanners. However, they have still highly unoptimized spatial resolution and therefore may miss small structures.

Currently (end of 2019/beginning of 2020) there are several existing dedicated brain PET imagers developed by small companies, several research systems were recently funded and are under construction, and few more systems are planned. What is

important, in the last group there are systems involving also large companies, who do not develop yet their own dedicated (or optimized for brain imaging) brain imagers but started to offer their latest PET technologies to their partners from academia to develop dedicated brain PET prototypes. This reflects the growing interest in imaging the brain with high precision, high sensitivity, and at the lowest possible radiation dose from injected radioactive imaging agents.

In addition, there are several imagers proposed by academic/government/private consortia in China with a couple of systems already funded and under construction, to be delivered in a short period of 1–2 years. Therefore, one can describe the competition as the quickly accelerating race to the market with the global multi-billion-dollar diagnostic neuro-market in mind. Diagnosing and even screening for and staging dementia, TBI, and cancer are at the top of the immediate areas of interest.

The near-future prospects are fascinating: approaching 1 mm resolution in the dynamic imaging protocol of the whole brain up to an order of magnitude higher sensitivity than currently possible. The detector technology that can achieve such outstanding performance already exists and the issue is how to implement it at a level of reasonable complexity and associated cost. Optimal reconstruction software is also a key. Plus implementing AI to assist with image analysis and interpretation. In fact, modern software can remedy limitations of the hardware design. This has a paramount effect on decreasing system's complexity, cost, time to develop and time to market.

The past attempts in designing dedicated brain PET imagers failed to offer high sensitivity and/or whole brain coverage, while demonstrating the potential for high resolution. This was primarily due to the initial cost of the high performing technology but also due to other added "distractions" like system's mobility and motion tolerance by imposing the limits on the weight of the scanner and, therefore, its stopping power and sensitivity to radiation.

The current generation of systems under design or construction can be somewhat arbitrarily divided into three groups: 1) high sensitivity by expanding angular coverage in the axial dimension, primarily by increasing the axial length from the usual 25 cm to 50 cm (the mini-Explorer–type cylindrical approach), 2) high resolution, pushing down towards the ∼1 mm limit, but at the expense of low coverage and/or low sensitivity and 3) compact-helmet–type 3D coverage to boost sensitivity in the whole brain, however still in the current implementations plagued with many breaks in angular coverage, causing an estimated loss of about half the potentially achievable sensitivity, when using such an extensive 3D coverage (example: the Yamaya's group effort in Japan [36-38]).

An interesting example of the instruments from group 1 above is the mini-Explorer system developed originally for animal research that may achieve high PET detection sensitivity *in the whole brain volume*, combined with very high spatial resolution, all in a robust well-tested traditional cylindrical design, that came as a spin-off from the development of the Explorer total-body imager (fig. 4). While mini-Explorer II is not approved for human use and is in fact slightly too tight for human use, it was used as the base for the proposed NeuroExplorer brain PET scanner (proposal submitted to NIH in October 2019). The high sensitivity in these structures is achieved through "brute force" increase in 3D angular coverage by using an extended axial length (∼50 cm) cylindrical detector structure. Close to an ideal system, on top of high sensitivity, it would also have a combination of excellent operational parameters such as ∼250 ps FWHM TOF resolution, and ∼4 mm DOI resolution, that combined with small scintillator pixel pitch would result in <2 mm FWHM reconstructed spatial resolution in the whole brain volume. The standard clinical PET scanners have typically two times shorter (∼25 cm)

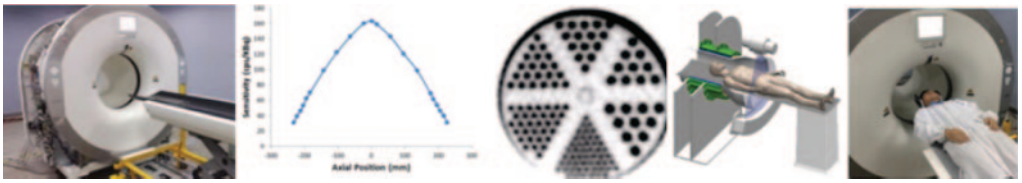

Fig. 4. – The mini-Explorer II [41] from United Imaging with about 50 cm axial length can be in fact used efficiently in brain imaging. The center-left plot shows the sensitivity profile. Center-right: Derenzo phantom image showing high-resolution performance. Rod diameters range from 3.6 to 1.6 mm. Right: diagram showing a human subject positioning for brain imaging and a volunteer positioned for mini-Explorer II PET scanning (picture kindly provided by Dr. Hongdi Lee, United Imaging).

axial length with smaller angular coverage in 3D, and have spatial resolution in the 3–5 mm region. Due to a much better spatial resolution, and thus improved Partial Volume Effect (PVE), an additional boost to detection sensitivity of small structures, lesions, etc. will be obtained. Such a very high performing system will also enable high-quality dynamic scans, typically limited by low-event statistics.

The special group of the dedicated PET brain imagers are the PET inserts in MRI [39, 40, 42-50]. They must be compact enough to fit inside the magnet bore and must be MRI compatible. A good example is the MindView PET brain insert [8, 46, 47] from Oncovision.

2˙2. *Restating the rationale.* – Potentially the main present-day motivator for high performing (high sensitivity and high resolution) dedicated brain imagers is "detecting Alzheimer's disease before it is too late". The dream is the Manhattan-Project–scale project to eliminate Alzheimer's disease by early detection, years before the disease is visible and becomes incurable. The research suggests that anti-amyloid, anti-synaptic damage, etc. therapies would be most effective before the patients reach the threshold for preclinical AD, and long before the first signs of memory issues set in. For that screening program to be successful we need at least:

- tens or hundreds (for scanning availability to thousands of patients) low-dose, low-cost high-sensitivity brain PET scanners to screen for dementia, and then monitor changes due to different treatment protocols;
- creation of specialized expert dedicated Alzheimer's Screening Centers to enable such a national/international scanning program (presently the established medical centers do not even have room for so many new scanners); there is an existing small-scale model of how to organize such an initiative: Amen Centers, but they use sub-optimal SPECT scanners with high doses of multi-mCi Tc99m labels in the imaging agents;
- create the Scientific Advisory Board for the network of Alzheimer's Screening Centers in order to coordinate the efforts and to expedite the program to find cure for Alzheimer's disease.

With Alzheimer's disease always being at the top of the short list of important brain diseases, TBI is however also a leading cause of death and disability among children and adults in the United States, it contributes to approximately one third of all injury-related

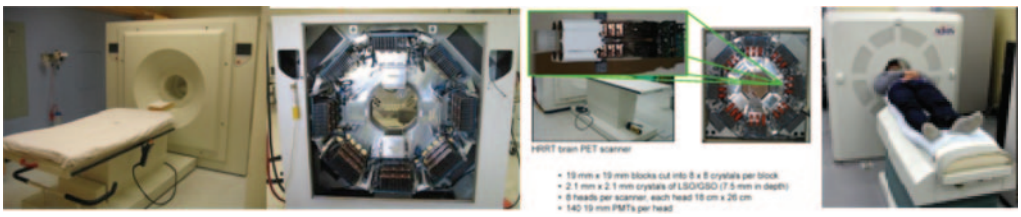

Fig. 5. – Prior art designs of the dedicated stand-alone PET brain imagers. Still the highest-resolution (as of today, 2019) dedicated brain PET imager: HRRT from Siemens [32-35]. On the right the jPET D4 research system is shown [1].

deaths and creates a staggering economic burden of over $ 76 billion annually. Each year an estimated 1.7 million Americans sustain a TBI and, since 2000, more than 300000 of these cases have occurred in the military alone.

Head trauma not only results in brain injury instantaneously, but also in secondary brain injury (SBI) that develops in a delayed fashion over a period of days to weeks. In medical terms, the disruption in integrity of cell membranes in neural tissue and in utilization of oxygen can have profoundly deleterious effects such as edema, ischemia, subclinical seizures as well as the so-called cortical spreading depolarizations. Current clinical assessments for these conditions are inadequate, so they often go undiagnosed and untreated, resulting in avoidable neurologic damage, disability or death. Universal treatment is not an option as TBI is dynamic and the course it takes in each patient is difficult to predict. It is crucial to know if, when and which type of these complications develop, as the treatments differ, and each treatment has its own set of risks. There is a critical need for a rapid, real-time method to identify complex, evolving SBI in TBI patients in the Neurocritical Care Unit, that can repeatedly assess metabolism in the whole brain, without having to move these unstable patients.

2˙3. *Selective approach to the review of the prior art.* – In recent years several reviews of the PET instrumentation in general [49,51-61] and of dedicated devices, and specifically of dedicated PET brain imagers, were published. Therefore, we will not attempt a historical and complete review of the field, but focus instead on the current relevant efforts and on the differentiation of our effort from other similar developments either finished or the recent and most relevant, that are in progress. In figs. 5, 6 we show a

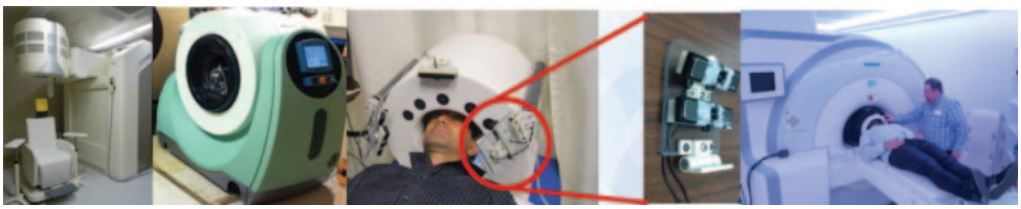

Fig. 6. – Few modern examples of the dedicated brain PET imagers. From left to right: Hamamatsu upright HiTPET imager (with patient sitting) [4,5]; the first built with SiPMs dedicated mobile brain PET; NeuroPET/CT from PhotoDiagnostic Systems (in package with CT) [3]; Cere-PET mobile brain PET with stereo-camera based motion head correction system [62-64], from Brain Biosciences; and MindView PET brain insert in 3T MRI [46, 47].

very short summary of the prior art in two figures with the special emphasis on Siemens HRRT, still the highest resolution brain PET imager [32-35].

3. – Simulations of the new designs

Developments in compact high-granularity PET technology with DOI capability [65-95], for example based on small animal PET scanner designs and after careful theoretical analyses of the detection phenomena in the detectors, permit now to design PET brain systems with high spatial resolution [96-113], however to be truly successful these designs must also provide high sensitivity.

In addition, to attain practical high resolution in the clinical system, and not just in static and dynamic phantom studies [114-119], robust motion correction systems will have to be implemented [62-64, 94, 120-146].

In recent years several papers were devoted to designs and simulations of the dedicated brain PET [36-38, 147-156] typically done in comparison to standard clinical PET/CT scanners and also to the Siemens HRRT dedicated brain imager [32-35], used as a key reference. The theoretical simulations, performed by several groups, have shown that tight idealistic detector geometries following the shape of the human head and furthermore with add-on top and under-the-chin or at the back-of-the-head detector modules, are boosting significantly the detection sensitivity, especially in the top and bottom regions of the brain (figs. 7, 8). These simulations also show that instead of using a given number of detector surface elements in a simple common diameter cylindrical geometry, one can rearrange these modules in a hemispheric shape and substantially gain sensitivity especially at the top of the brain. While the cylinder can be well approximated in practice with the set of rings, the hemisphere is very difficult to cover with planar modules of fixed sizes and with many accompanying cracks that are left in-between the modules.

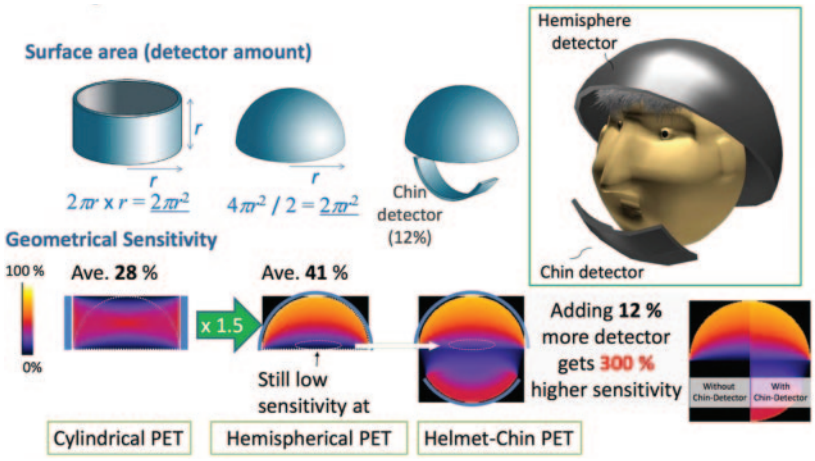

Fig. 7. – Idealistic simulations of the tight helmet type brain PET imager: Helmet-Chin PET (from Yamaya *et al.* [36-38]) assuming idealistic geometrical sensitivity distributions for the cylindrical PET (a), helmet PET (b), helmet-chin PET (c). The cylindrical PET and the helmet PET had the same assumed detector surface area and the helmet-chin PET had a 12% increase in the total detector surface area. One can notice how little improvement in the brain the narrow chin detector adds.

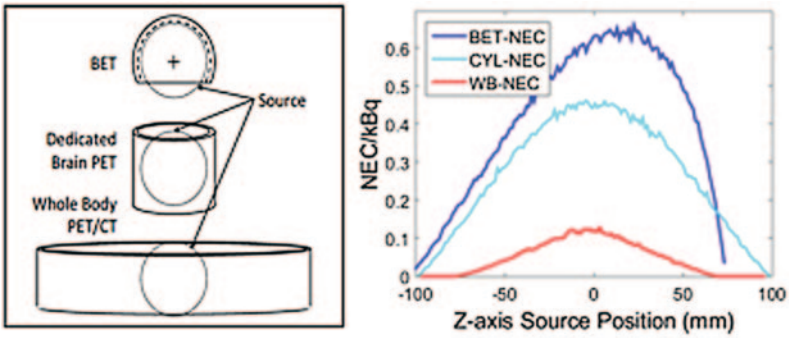

Fig. 8. – Another idealistic (Schmidtlein *et al.* [150,151]) three-way comparative simulation study between the spherical (BET), cylindrical (CYL) and whole-body (WB) type PET structures (left). A simple water sphere of 20 cm diameter was assumed as the head. 25 mm of LYSO scintillator was assumed in each case. The three curves on the right are the Monte Carlo predicted NEC responses with inclusion of scatter effects along the central axis from chin to top of the head. The compact cylindrical structure is seen as giving performance approaching the performance of the optimal sphere design.

And in fact, even in the simple long cylindrical structures built with practical modules, while solving the major issue in angular coverage, breaks still remain between the modules in the rings forming the cylindrical structure of the detector.

Schmidtlein *et al.* [149, 150] performed a three-way comparative simulation study between the spherical, cylindrical and whole-body type PET structures (fig. 8). A simple water sphere of 20 cm diameter was assumed as the head. A 25 mm thick LYSO scintillator was assumed in each case. The Monte Carlo calculations predicted NEC responses with the inclusion of scatter effects. The compact cylindrical structure was discovered as giving performance approaching the performance of the theoretically optimal spherical design.

In the framework of the AMPET project (`www.pethelmet.org`) several designs of the helmet PET detector were simulated [148] (fig. 9). Specifically, the effects of added top and chin region modules were investigated, following the work of Yamaya *et al.* [36-38]. The selected special, shown below, helmet shape increases mean sensitivity by an average

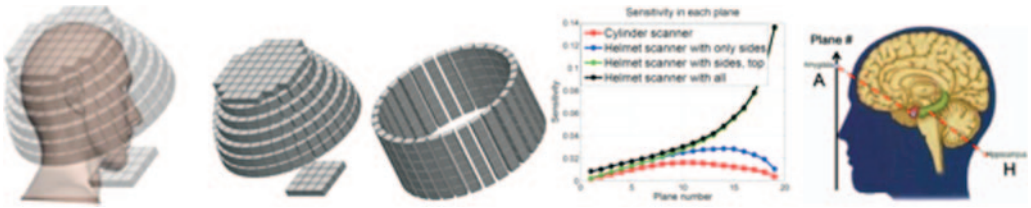

Fig. 9. – Selected results of the brain PET simulation study in the framework of the AMPET project [148], comparing a helmet-type PET scanner with top and chin modules (left) with a simple cylindrical structure (third from left). In this simulation modules with ∼3 cm square cross-section were used. The results (in the plots in the second panel from the right) demonstrate that the sensitivity of the scanner benefits already from a structure following the shape of the human head (blue curve *vs.* red curve). The key increase of the sensitivity is produced by adding the top detector panel (light green curve). The module under the chin boosts the efficiency in the lower regions of the brain, such as amygdala (A) and hippocampus (H).

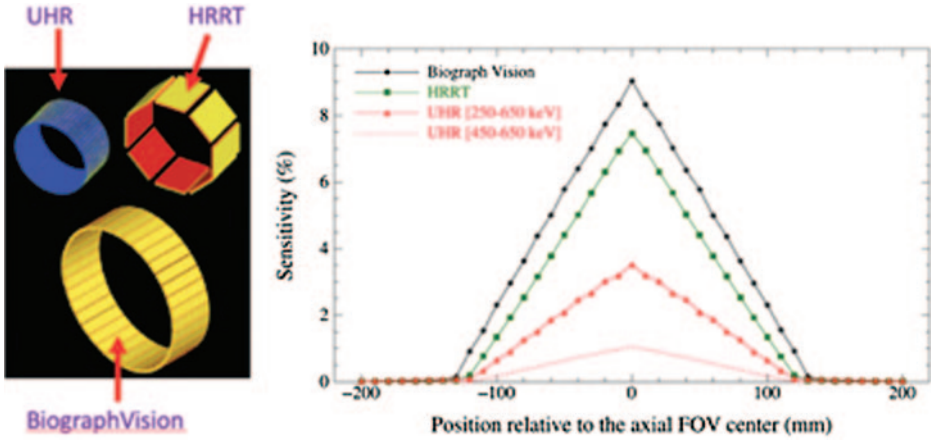

Fig. 10. – Axial sensitivity profiles for the MGH/Sherbrooke proposed Ultra High Resolution (UHR) imager calculated for two energy windows of 250–650 keV and 450–650 keV, and compared to the HRRT and the Biograph Vision scanners, when used with their corresponding standard energy windows [156].

factor of 4 compared to the standard PET scanner, with most of the increase in the upper and lower parts of the brain and rather little impact in the horizontal midline regions. These results strongly indicate that it is indeed important to follow the shape of the human head as much as possible.

As one of the special simulated systems selected for the purpose of this limited review, the Sherbrooke/MGH team is building a ∼1.3 mm resolution dedicated compact brain imager [156] (fig. 10). They propose to design and build this next-generation PET scanner for ultra high resolution imaging of the human brain using hardware advances developed by members of their collaborative team to achieve unprecedented Spatial resolution Approaching *in Vivo* Autoradiographic Neuro Tomography (SAVANT) performance, with high count rate capabilities. The system will have a volumetric resolution close to 1 mm^3

Fig. 11. – Few examples of other discussed multi-modular helmet structures using smaller detector modules in an attempt to follow closer the shape of the human head. The example on the left is the recent example of a possible implementation of the helmet concept using smaller modules, from Yamaya *et al.* [36-38]. This particular implementation also includes a bottom detector portion placed under the chin. However, all these new approaches introduce many more albeit smaller breaks and cracks in the angular coverage. On the right the very recently proposed structure by Catana *et al.* is shown; this initial concept shows a complicated module arrangement with many cracks in active coverage. Also note that these sketches do not take into account the complicated cabling issues, space needed for the cooling systems tubing, etc., when considering such multi-modular structures.

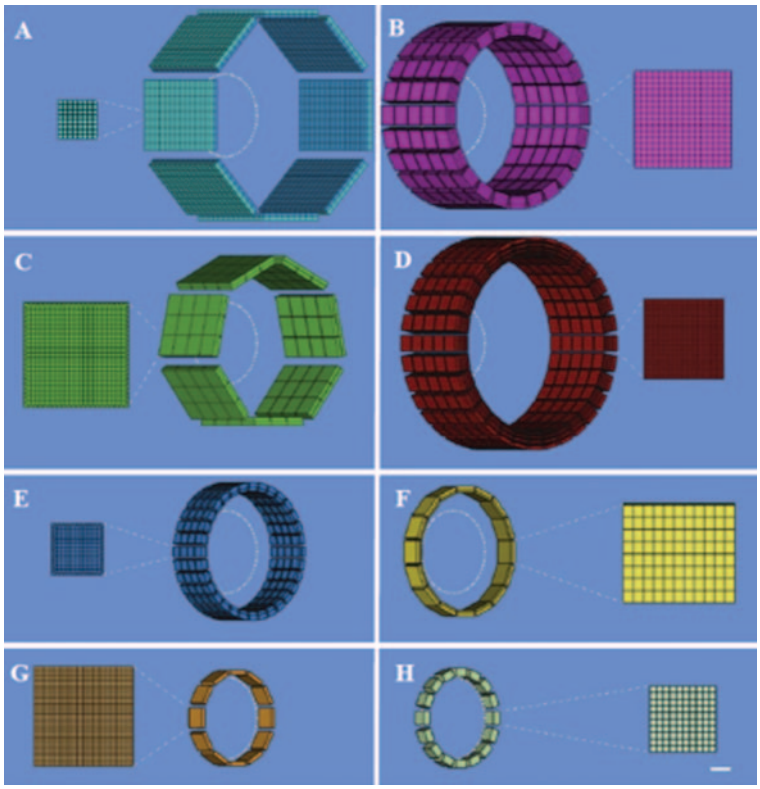

Fig. 12. – Examples of recently simulated detector configurations [157]. Dedicated PET scanners with conventional geometries: (A) HRRT, (B) jPET-D4, (C) NeuroPET/CT, (D) Hamamatsu, (E) BBX, (F) PET-Hat, (G) Helmet-PET, and (H) Mind-Tracker. A 20 cm diameter circle is shown inside each scanner. The scale bar represents 1 cm in the detailed views.

(isotropic spatial resolution close to 1 mm), which is approximately 27-fold better than the best dedicated brain PET scanners and 125-fold better than general-purpose PET scanners. Such a major improvement will allow visualization and quantification of *in vivo* physiological events as never before possible, for example in the entorhinal cortex in the early stages of Alzheimer's disease and the dopamine transporter concentration in the *substantia nigra* area. This will allow the detection and quantitation of brain disease at a much earlier stage, decades before the onset of clinical symptoms, and permit the study of key structures in neurotransmitter systems that currently cannot be imaged accurately with PET. The proposed high-resolution PET scanner will be validated in phantom studies and performance evaluated in healthy volunteers.

The very recent and relevant reference is the Brain Initiative funded project proposed by Ciprian Catana from MGH to develop technology for the PET helmet imager insert for the 7T Siemens MRI [157] (figs. 11, 12). The authors propose "A possible spherical geometry that would maximize the solid angle coverage. In this case, the PET detectors with DOI capabilities are arranged around a partial-sphere (32 cm inner diameter) with a 25 cm diameter front opening to allow the positioning of the subject (wearing MR-compatible goggles to maximize comfort and display stimuli) and a 9 cm diameter

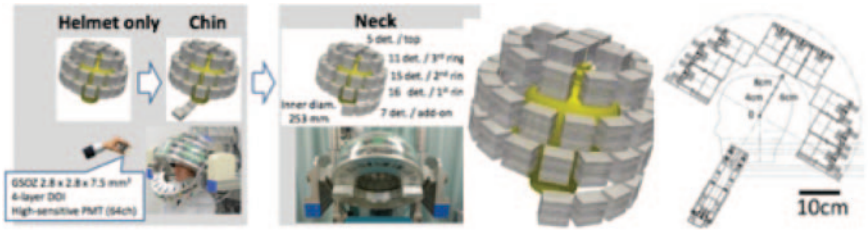

Fig. 13. – Key examples of practical systems developed to approximate the ideal helmet shape, in order to achieve optimal brain imaging. Practical realizations of the Helmet-Chin PET and Helmet-Neck PET prototypes from Yamaya *et al.* demonstrate the engineering issues encountered when working with arrays of practically sized modules [36-38]. While theoretical simulations and comparisons are made using idealistic assumptions about the possible shape and ignoring the breaks in sensitive area coverage by the detector, the presence of many physical breaks in the coverage can be easily recognized in practical prototypes, due to the challenge of placing the detector modules tightly in 3D, as well demonstrated on the right, where the many residual gaps in angular coverage can be appreciated.

back opening for the cables. The estimated solid angle coverage for this configuration is ∼71%. Assuming 90% 511 keV photon detection efficiency (for 2.6 cm long lutetium oxyorthosilicate crystals) and 40% scatter fraction, this translates into ∼25% sensitivity for detecting true coincidences. Furthermore, after considering the virtual sensitivity amplifier of including the time-of-flight information, the effective sensitivity of this scanner could be as high as 50%, a dramatic improvement compared to current values".

4. – Examples of the prototype research helmet systems

Examples of systems developed to approximate the ideal helmet shape, in order to achieve optimal brain imaging, are shown in figs. 13, 14.

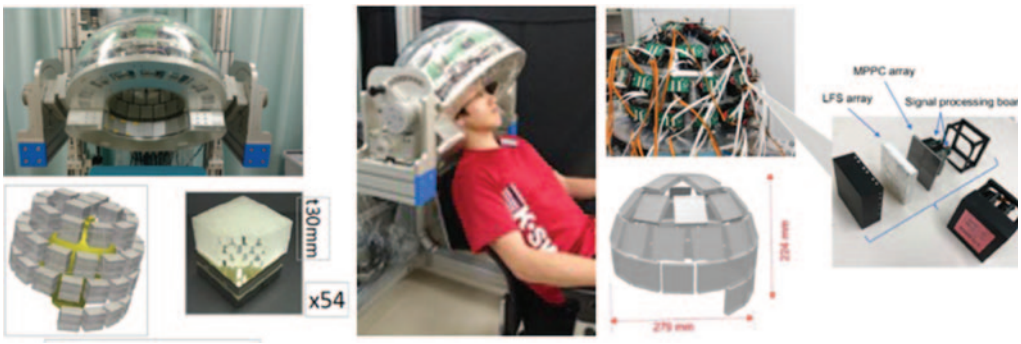

Fig. 14. – The multi-modular practical designs approximating the spherical shape have many breaks in coverage, even when using intrinsically very compact SiPM technology. Examples above are shown from Yamaya's group [36-38]: (left) PSPMT-based modules, and (center) based on SiPM modules. The coverage improved with SiPMs (smaller gaps) but still many gaps remain.

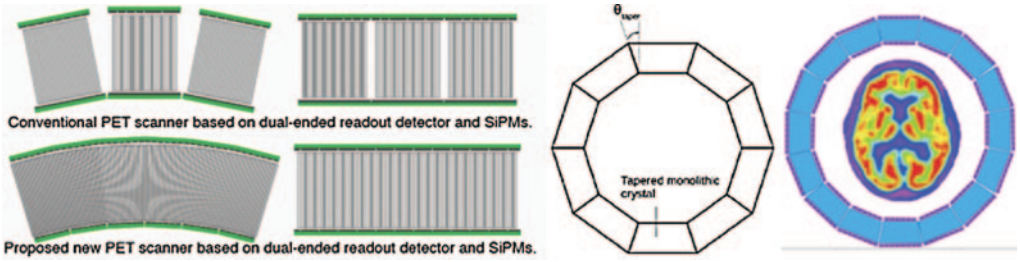

Fig. 15. – Examples of reducing the gaps/dead spaces between detector modules in the pixelated and monolithic versions. On the left the UC Davis design is shown (Du *et al.* [112, 113]). In the center we show the design using a ring of glued together monolithic scintillator modules (suggested first in the paper by Vinke and Levin [158]). Gluing, while creating challenging readout issues due to scintillation light propagation, eliminates the trans-axial breaks in the coverage. To improve performance, the SiPM readout could be in principle attached at both ends of the monolithic scintillators, at a cost of complicating the design and increasing the cost.

5. – On the path of closing the coverage gaps

As discussed before, it is very difficult to follow the idealistic geometrical prescriptions when implementing arrays of standard planar-shaped modules arranged in a 3D pattern with many mechanical breaks between the modules. As a result, the ideal shape is poorly approximated by the achieved pattern with many breaks with missing solid angles in coverage. Depending on the particular design, one can estimate that the loss in angular coverage can reach almost 50%.

As noticed by several groups, the breaks or gaps between the modules can be minimized or even almost eliminated by introducing a continuous active detector medium, either filled with tight arrays of converging scintillating fibers (example: Junwei Du, UC Davis [112, 113]) or with glued arrays of monolithic scintillators (the idea based on the original concept from Craig Levin, Stanford [158]) (fig. 15).

Fig. 16. – Recent ideas using monolithic scintillator pieces that started to address the issue of cracks in angular coverage through decreasing the gaps between detector modules by placing scintillator edges close to each other. Left: dodecahedral (drawing courtesy of Qiyu Peng, LBNL, Berkeley, CA). Center: similar but more open small gap design using 10 cm squares and triangles (image courtesy of Jose Maria Bennoch, i3M, Valencia, Spain). However, while the physical gaps are getting smaller, and there are fewer of them, there are still optical barriers between scintillation pieces, creating discontinuity effects and gaps in image quality and even image artifacts due to the performance gap regions at the mechanical joints. On the right, for comparison, we show the Italian (courtesy of Franco Garibaldi, INFN, Rome) conceptual SiPM-based design, also showing many physical cracks in coverage.

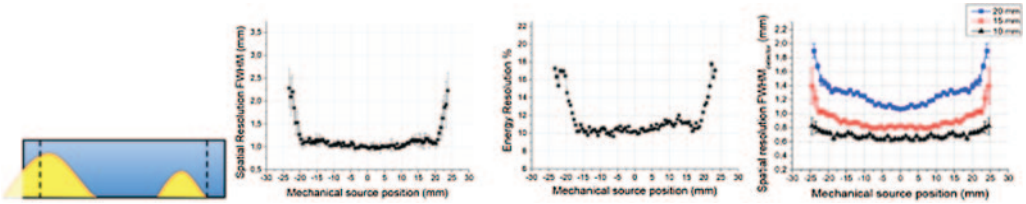

Fig. 17. – Example of the edge effects encountered when using monolithic crystals. Left: illustration which shows that scintillation light is truncated at the edges, and the effect gets worse with increasing scintillator thickness and increasing distance from the exit (bottom here) surface on its way to the photocathode. Center: example of the impact on the spatial resolution and energy resolution in a 5×5 cm cross-section $\times$ 10 mm thick LYSO crystal. Right: even using optimized readout/reflector schemes provides only limited improvement. Detector intrinsic spatial resolution FWHM as a function of the source mechanical position. Black full triangles show the results for the 10 mm thick crystal, the red open circles those for the 15 mm thickness and blue full squares are for the 20 mm thick [178]. The edge effects are, as expected, indeed stronger in thicker crystals.

The monolithic solution is well established [158-180] and there are several systems built using monolithic scintillators for small animals and brain imaging, and the technology is also present in products, for example in Oncovision's brain PET CareMiBrain and MindView scanners. In the monolithic variant, without optically joining the pieces at the edges, while otherwise operating with good signal response and with very high DOI resolution and planar resolutions in the central parts of the detector modules, the response of the detector becomes highly non-linear and non-uniform when approaching the scintillator monoliths edges as the process of the scintillation light spread in the monolithic crystals becomes more and more truncated and distorted when approaching the edges (figs. 16–18). Even with optimized spatial algorithms the signal deterioration effects are clearly manifested in the loss of energy resolution and spatial resolution at the edges of the scintillator pieces. As a result, the overall detector response is highly non-uniform with the regularity of the module spacing and the edge effects dominate its performance and ultimately lower the detection sensitivity.

In the quest to maximize sensitivity, the optimal designs should eliminate the multiple cracks in the angular coverage of the standard multi-modular structures, by building the scanner from optically glued arrays of monolithic scintillator modules, using the high refractive index optical compounds (figs. 19–21). The adjacent modules will have optically coupled surfaces, both between the neighboring modules in the rings, and between the neighboring modules in different rings. In the cylindrical/multi-ring part, the scintillator modules will have tapered shapes. For example, three rings of 16 modules each can form the cylindrical part, while 3×5 and 5×5 optically coupled planar module arrays can be installed in the bottom and top panels, respectively, closing the structure in 3D. The previous designs had breaks in physical coverage (with the accompanying loss in sensitivity) due to the gaps between the individual modules in a ring and between the rings in the standard multi-module helmet designs. In comparison, the previously discussed mini-Explorer approach uses an extended and shrunk in diameter PET scanner cylinder, compared to the whole-body clinical PET scanners. Due to that structure, the obtained sensitivity in the mini-Explorer is lowered in the top and bottom regions of the brain, compared to the center.

In a paper by Vinke and Levin [158], the solution was proposed of how to build a continuously sensitive detector by optically coupling tightly fit monolithic scintillator pieces. With properly selected optical compounds with high refractive index, scintillation light will be shared in the border regions and not bounce back due to total internal reflection, resulting in the fully active scintillator volume. Based on their simulations, the authors concluded that with the optical coupling scheme good spatial linearity and resolution can be achieved at the edges of optically interconnected monolithic crystals. With this technique, monolithic scintillation detectors can provide good positioning and timing performance at reduced complexity compared to current detectors used in clinical whole-body PET, and offer a cost-effective solution for measuring DOI.

The study by the Seattle/Pisa group [171] experimentally confirmed some of the optical coupling concepts. A semi-monolithic crystal assembly was formed using four 26 mm × 26 mm × 10 mm LYSO crystals optically coupled together using optical adhesive, to mimic a 52 mm × 52 mm × 10 mm monolithic crystal detector. The obtained large scintillator block was coupled to a Multi-Channel PMT. The key conclusion from that experimental study was that the spatial performances of a module composed of a multi-channel PMT coupled to 4 optically coupled crystals only slightly degrade near optically coupled interfaces compared to a single monolithic crystal read out by the same photodetector array. Degradation of the performances near optically coupled quadrant interfaces is much less than degradation at the external edges of the detector. The authors conclude that the adoption of optically coupled crystals for a PET detection system composed of monolithic scintillators can be a useful and feasible method to improve the uniformity of performances in the whole sensitive area.

6. – Role of TOF in increasing practical sensitivity

TOF performance is, after stopping power and angular coverage geometry, another key parameter impacting system's sensitivity [181-187]. TOF capability in PET imaging adds an ability to locate the point of annihilation more precisely along the line of response (LOR). Good TOF capability improves detection sensitivity via improved S/N in the 3D reconstruction process due to removal of overlapping signal coming along the same lines of response (LOR). In addition, the excellent TOF resolution assuring high signal-to-noise

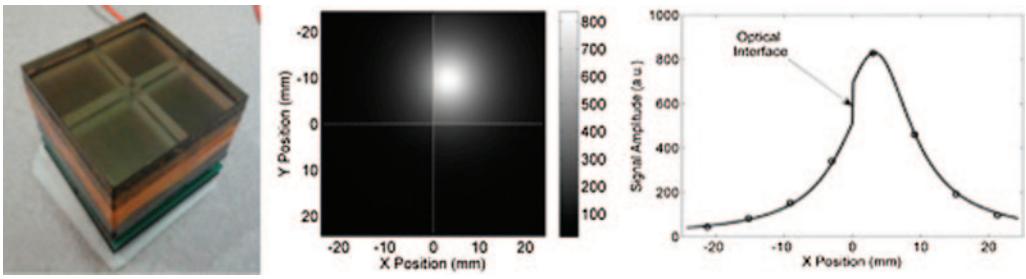

Fig. 18. – Experimental demonstration of the ensemble of four glued scintillator by the Pisa/WashU group [171]. Left: picture of the four-component pseudo-monolithic crystal optically coupled to the multi-channel PSPMT. Example of the light distribution on the 64 channels of the PSPMT, followed by a multi-Lorentzian curve obtained by the fit of the measured distribution. Right: profile of the light distribution on the third row of the PMT and profile of the fit on the same Y (vertical) position. Note only a small residual discontinuity due to the crystal-crystal interface (arrow).

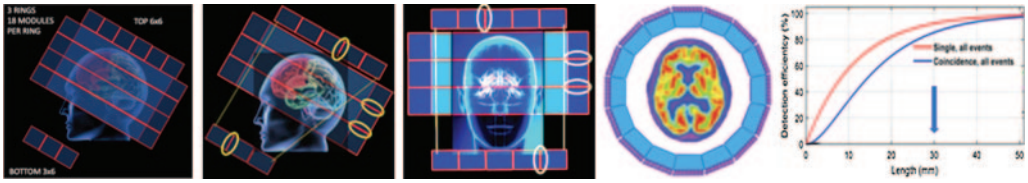

Fig. 19. – One of the proposed novel brain PET concepts. In the quest to maximize sensitivity, this novel design will eliminate typically present multiple cracks in the angular coverage of the standard multi-modular structures, by building the scanner from optically glued arrays of monolithic scintillator modules, using the high refractive index optical compounds. The yellow ellipsoids highlight few selected examples of adjacent module junctions with the optically coupled surfaces, both between the neighboring modules in the rings, and between the neighboring modules in different rings. In the cylindrical part, the scintillator modules will have tapered shapes, as shown schematically on the right. For example, three rings of 16 modules each can form the cylindrical part, while 3×5 and 5×5 optically coupled planar module arrays will be installed in the bottom and top panels, respectively, closing the structure in 3D.

ratio (SNR) and the increase in sensitivity eliminates also the necessity for accompanying CT or MRI images to provide attenuation correction, as the attenuation correction can be obtained from the same PET scan [188-195]. In fact, the dedicated TOF PET brain scanner does not require any additional structural information to provide fully corrected reconstructed images. It is indeed a stand-alone system. Plots in fig. 22 show the dependence of the signal to noise (S/N) on the FWHM TOF resolution of the scanner in detection of several structures. The advantage is most pronounced for the full human body but even just for the head the improvement at 200 ps FWHM is calculated as a factor 2.5 when compared to the non-TOF case.

Robust TOF resolution (less than 300 ps FWHM) can serve as an important sensitivity enhancing parameter [196]. Several studies estimate a factor ∼4 sensitivity increase compared to a non-TOF system via an improved SNR when imaging an object the size of a head (20 cm) in a PET system with 300 ps TOF resolution (see plot below).

However, good TOF performance is achieved through special detector module design [197-206] with utilization of fast photodetectors [207-217], fast scintillators [218-222]

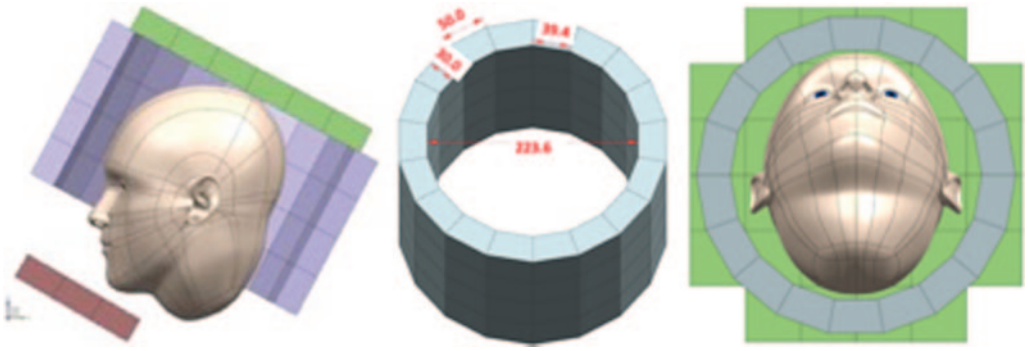

Fig. 20. – Initial design of the scintillator helmet made from glued pieces. Center and right are sketches of the 3-ring cylinder, each cylinder in this example made from 18 modules, and a planar top panel made from 32 glued modules. (Sketches kindly provided by Jose Maria Benlloch, i3M, Valencia).

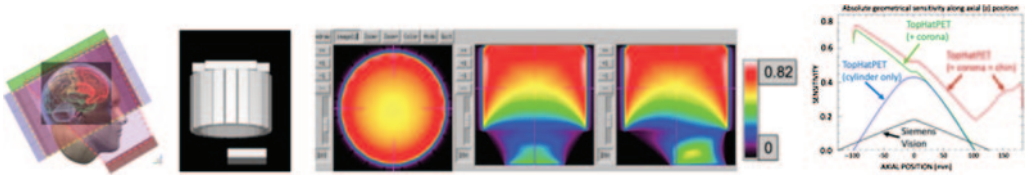

Fig. 21. – Graphical rendering of a simulated model for the Top Hat PET scanner. Center: three views (top, front and side) of preliminary sensitivities with a color scale shown in the scale bar. The importance of added top and bottom panels in increasing the sensitivity, especially at the top of the head where most of the brain resides. The Top-Hat PET geometrical comparative simulations show that a factor 2–3 in sensitivity increase compared to Biograph Vision is possible (Johan Nuyts, Loeven, private communication).

and fast timing electronics [223, 224] and digital readout [225-231], that typically is more bulky and power consuming and often requires cooling. Detectors for TOF PET are also required to have high photon detection efficiency (PDE), good energy resolution, good spatial resolution, and excellent timing resolution.

The variance reduction of a TOF-PET system over a non-TOF PET system can be computed analytically for the center of a uniform cylinder and, assuming $D \gg \Delta x$, it equals

$$\frac{VAR_{nonTOF}}{VAR_{TOF}} = \sqrt{\frac{2\ln 2}{\pi}}\frac{D}{\Delta x},$$

where D is the diameter of the cylinder and Δx is the TOF spatial resolution. Therefore, the variance gain of one TOF-PET system over another is inversely proportional to the ratio of their TOF resolutions (fig. 22). Consequently, a brain PET system with 100 ps TOF resolution achieves a four-fold variance reduction over a system with 400 ps TOF resolution. To achieve such a record consistent systemic TOF performance, the crystal thickness may need to be lowered. However, as an example, reducing the crystal thickness from 2.5 cm down to 1 cm will reduce the stopping power for a photon pair by a factor of approximately 2.3, increasing the variance of the same factor. This would offset part of the variance improvements mentioned above due to improved TOF. The new frontier of 100 ps FWHM was already defined as the next goal [232]. An even better TOF advantage will be obtained at 50 ps CRT once this value, as planned, will be achieved in a few years. The latest developments in SiPMs and fast readout make this vision quite possible [233-239].

With the above described variance estimation technique, the variance gains associated with design choices can be computed more accurately at particular locations in the brain, for specific tracer distributions and imaging tasks.

In addition, the excellent TOF resolution assuring high SNR and the increase in sensitivity eliminates also the necessity for accompanying CT or MRI images to provide attenuation correction, as the attenuation correction can be obtained from the same PET scan [188-195]. In fact, the dedicated TOF PET brain scanner may not require additional structural information for each scan to provide fully corrected reconstructed images. It could be indeed a stand-alone system.

An interesting new direction in TOF PET is the exploitation of the Cherenkov light emission in BGO. Traditionally this slow and not so bright scintillator had the only

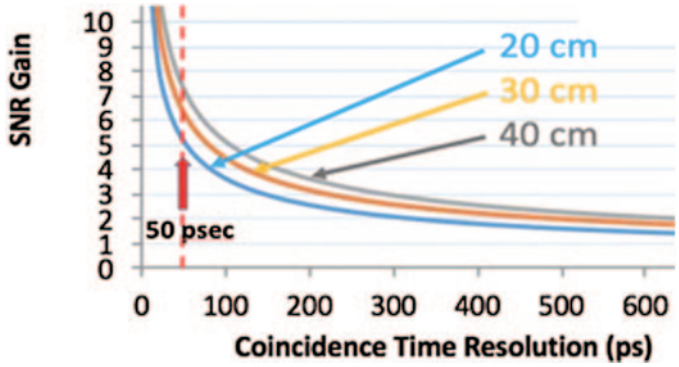

Fig. 22. – Advantage provided by TOF. SNR improvement as compared to non TOF PET system as a function of the time resolution for different diameters of the FOV with 20 cm being representative of the head [233].

advantages of being low cost and free of natural activity from radioactive nuclei in its material [240-242]. Benefiting from an efficient production and prompt emission of the Cherenkov light in BGO, this slow scintillator may one day achieve systemic 300 ps or less FWHM TOF resolution. In small BGO samples coupled to new improved SiPMs equipped with fast electronics TOF values below 200 ps FWHM were obtained in laboratory studies [243-245].

In addition to Silicon Photomultipliers (SiPMs), Large-Area Picosecond Photon Detectors, large-area economical Microchannel Plate Photomultipliers (MCP PMTs) are being studied as another means of lowering the cost of the TOF PET detector [246].

7. – Extraction of cardiac input function for kinetic brain imaging

From the extended published prior evidence it can be concluded that to perform accurate dynamic brain PET studies with the subsequent kinetic modeling and then parametric K maps, one needs a high-quality cardiac input function definition. There are several options: a) directly taking and analyzing blood samples (that is an invasive albeit gold standard method); b) from the images in the brain tissue (with some modeling); c) from cardiac aortas and/or left ventricle, etc.; or d) from carotid arteries (figs. 23, 24). Each of these options has its own challenges and their relative merits were not yet fully studied. Volunteer data from the total-body coverage uExplorer at UC Davis were used in the performed preliminary analysis with ROIs drawn in several of the candidate regions to perform simultaneous comparative analysis of TAC curves (study performed at UC Davis by Elizabeth Li). The extracted kinetic model results and K values using these ROI regions were compared to the available published data (no blood sampling was performed as part of the uExplorer protocol). To quickly summarize the pilot results, the cardiac aorta provided the most accurate values in agreement with the previous published data, while carotid results were off. The possible explanation is that to extract accurate signal from the carotids, ideally one should have a sub-mm spatial resolution imager. The resolution achieved in uExplorer of about 3 mm FWHM is not sufficient. The system of blood vessels in the neck is very complicated, and it is not easy to model and to overcome the partial volume effect. Therefore, one could use a dedicated neck PET imager with sub-mm spatial resolution to extract an accurate cardiac input function for

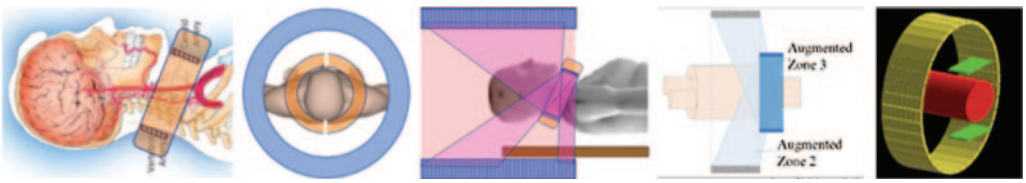

Fig. 23. – One possible solution considered for the mini-Explorer type brain PET: ultra high resolution small ring assembled from two half-rings placed on the left and right side of the neck will provide large angular coverage with only few breaks, as compared to the WashU/Siemens "outsert" solution [247], shown on the right, with three marked separate groups of coincidence events. In a tight full-angle coverage geometry, the additional contribution of the mixed coincidence events will be much lower. Therefore, the carotids' imager can operate as a separate unit.

dynamic brain imaging. This additional neck imager can be used as a companion imager in many brain imaging protocols, also including the ones obtained with standard clinical PET/CT scanners. With proper time-stamping, accurate time correlation between the two imagers can be achieved. Another option is to implement a cardiac aorta imager.

Benefiting from the recent availability of the total-body uExplorer PET scanner at UC Davis, the comparative simultaneous extraction of the input function signal from the recorded patient data from several regions including carotids, left ventricle, and aortas was performed. The obtained results showed that K_i parameter values obtained based on input function extracted from carotids were not accurate (when compared to the K_i data published in the literature) and that in fact the best ROI for image derived input function (IDIF) operation is the descending aorta, placed behind the heart and least impacted by heart motion, compared to other parts of the heart, and especially to the (pumping) left ventricle.

Based on these results from the uExplorer scans at UC Davis, and analysis of the data in the published literature, one may consider two main ROI regions to extract the IDIF needed for kinetic analysis of the dynamic brain scans obtained with the dedicated brain PET imager: 1) carotids, and 2) heart aortas (arch, ascending or descending).

As the main issue with extracting the signal from carotids is their flexible, irregular shape, motion and in general small cross-section, additionally adding to the Partial Volume Effect (PVE) [248-252] one would need to consider designing a very high resolution (approaching 1 mm FWHM in reconstructions) ring shaped detector, taking example from the small animal PET designs. However, even after this improved design, we are still facing the relative motion issues and overlap from other blood vessels in the neck. Very accurate motion correction of these small vessels will need to be maintained throughout the duration of the scan. In addition, such an imager will be in the visible volume of some brain PET designs such as the NeuroExplorer, interfering with imaging by the brain imager and introducing additional scatter into it.

8. – Imaging in motion

8˙1. *Neuroscience rationale.* – To this day neuroscience was not able to image the brain in the realistic human life situations. Imaging of the brain during real-life upright activities, starting from sitting with limited head motion to walking quasi-freely in the virtual/mixed and even size-limited real world, was not possible. If we could image the

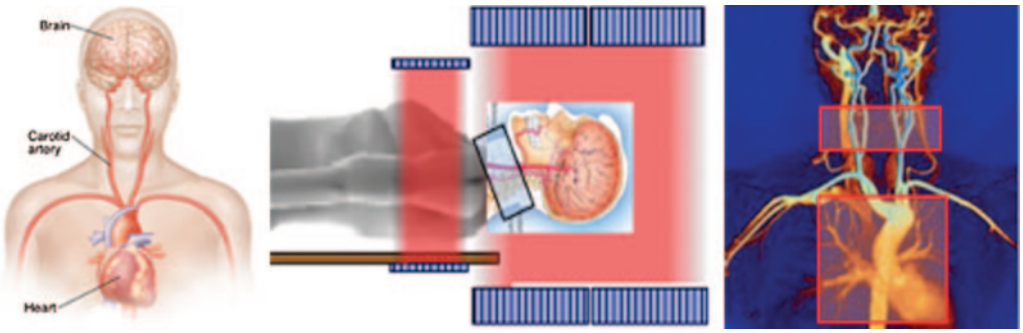

Fig. 24. – The cardiac input function can be measured from carotids or from several regions in the heart region. The NeuroExplorer brain imager, being developed by the consortium of UC Davis, Yale and United Imaging, is shown schematically.

whole brain while moving in a natural environment, we would be able to better understand the mechanisms behind our complex behaviors and how these change for different people and under different circumstances. We want to understand how the brain mediates a variety of complex behaviors, and to image humans immersed in real or realistic upright VR/AR scenarios. The standard relevant functional imaging modalities for imaging in humans, fMRI and PET, were requiring the patient/subject to be largely immobilized in a horizontal and therefore not natural position during most real-life activities, outside sleep (like walking, navigating and keeping balance). The ultimate goal is imaging of the human brain during realistic activity scenarios with a mobile "head-following" low-dose PET scanner. Such a dynamic motion-tolerant brain imaging system can give a never before possible insight into how brain operates in realistic conditions and be, for example, used in assessing the brain function in drivers, pilots, police, and the military, especially when under stress.

8˙2. *Wearable mobile brain imager: PET vs. other functional upright brain imaging modalities*. – The goal is to devise a brain imager that can image subjects being upright and "free to move around". The level of motion freedom is therefore one of the key parameters that must be considered. From the list of available functional brain imaging modalities, fMRI, MEG, EEG, fNIRS, and PET, only MRI and PET can reach deep into the brain, and only PET can make functional images of the whole brain of a person in an upright position. In addition, fNIRS scans are highly motion-intolerant due to delicate optical couplings between the emitters, receivers and the scalps of the subjects. This limits the studies to sitting position with very limited head motion. MEG is being developed in a wearable variant but is very sensitive even to the Earth magnetic fields [253]. In contrast, PET gives very robust signals and is not sensitive to electromagnetic environment. In principle, the subject can stand up and walk away. However, the issue with PET is the need to carry the weight of the imager, that can reach 10 kg and more, and the solution could be a robotic support.

It is important to note that the modern PET instrumentation based on solid state technology is a very robust, noise-resistant and intrinsically MRI compatible technique, that can be in principle paired with EEG, fNIRS or MRI (once upright fMRI is developed). However, as summarized before, none of these other techniques can withstand the requirement of upright motion tolerance beyond the sitting position with very limited head motion.

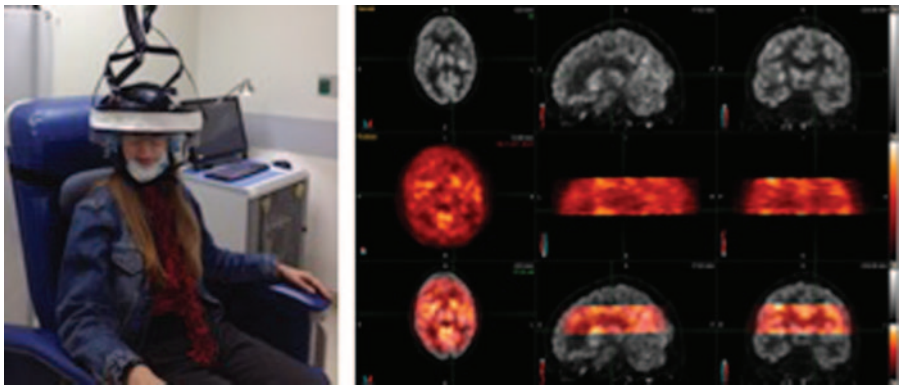

Fig. 25. – Helmet_PET [10-12], an upright wearable brain PET with limited axial field of view, allowing for wide head motions. On the left a picture is shown of a sitting volunteer wearing the Helmet_PET detector ring and showing that the PET imager moves with the head even during wide-angle movements. The imager has a limited ∼5 cm vertical FOV. Right: the pilot result of FDG brain imaging in a volunteer patient, compared to images obtained with the standard Siemens PET/CT. The images from the dedicated Helmet_PET are overlaid on the CT images from the PET/CT scanner.

The revolutionary concept of a wearable brain PET as the novel unique imaging tool to assess brain activity during realistic tasks (like standing or walking, social interaction, etc.) has many challenges preventing it from becoming fully or even optimally implemented (figs. 24–26). This is due to the basic conflict between the requirements of compactness, lightweight design, wearability with freedom of motion on one side, and high operational performance (specifically sensitivity, field of view) on the other (figs. 27–29).

One may imagine the next-generation revolutionary concept of a very high-

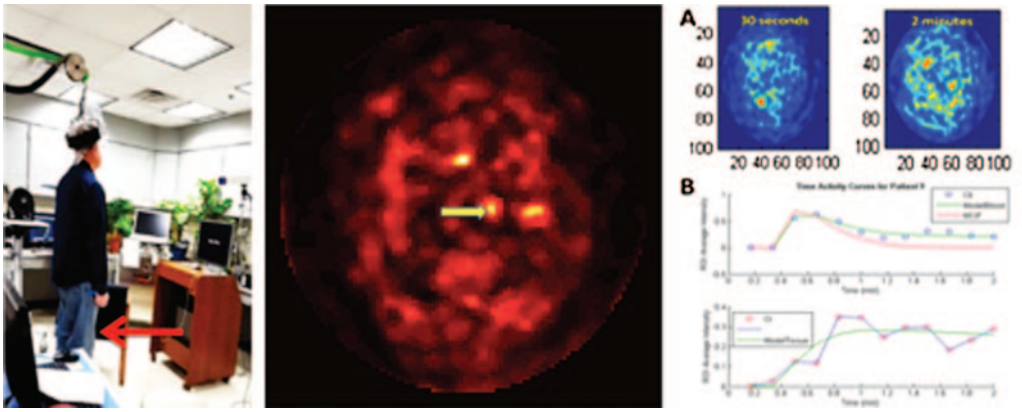

Fig. 26. – Imaging of the top 4 cm section of the head in the walking experiment, showing selection of the ROI regions for dynamic curve analysis. On the right we show the image used to select the carotid artery (marked with yellow arrow) for input function determination. Demonstration of the analysis using 3-compartment FDG Kinetic Model with formalism developed in the Bijoy Kundu Lab at the University of Virginia simultaneously computed the kinetic parameters and the model corrected blood input function (MCIF) from dynamic FDG images of the brain.

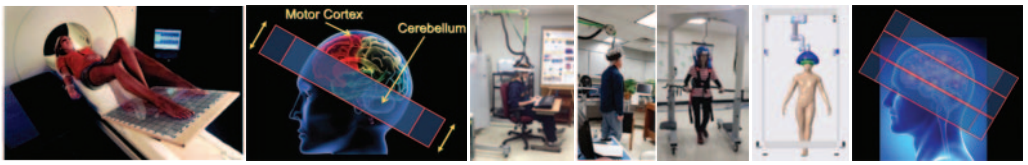

Fig. 27. – Depending on the brain imaging task, several models of motion-tolerant upright scanner can be used in brain engaging mobile tasks. From the simple, maximum mobility/limited brain volume imaging system to the more and more performing systems with increasing coverage and sensitivity, and higher demand for mechanical assistance, including finally the use of intelligent motion sensitive mechanics with robotic arms. In contrast, in the standard PET/CT scanner the subjects need to be in a horizontal position and mostly immobile, with only limited allowed motions of their extremities, as shown on the left. The mobility trajectory of the Helmet_PET [10-12]/AMPET [148] scanner is shown, with increasing weight and sensitivity. From sitting to standing, to walking in place, to walking with pushed/pulled mobile Biodex upright frame support using counterbalanced weight support (West Virginia University), and finally to robotic supported mobile system (sketch kindly provided by Professor Peter Kazanzides, Johns Hopkins University).

performance motion-tolerant brain PET imaging system based on robotic assistance, and benefiting from the "compression" of the real-world physical space into a relatively small "VR space" by using VR/AR environment designed to simulate many aspects of the real-world experience [13]. By substantially reducing the physical space and engineering requirements one can much better control the mechanical challenge associated with the implementation of the motion-tolerant high-performance PET scanner and optimize its performance, that otherwise would have been substantially limited due to mechanical restrictions and safety considerations. In addition, the VR/AR environment will create controlled and repetitive stimuli to study the brain under the same environment, which are typically very difficult to create and control in the real world. The key challenge is how much the "compressed world" can represent the real world. In fact, this will be an important part of necessary research to establish and improve this equivalency. In addition, such imager should be equipped with the cutting-edge dynamic/kinetic analytical algorithms on a par with the standard non-mobile systems to maximize its diagnostic power.

9. – Intrinsic conflict between the sensitivity and motion tolerance in PET and the paths forward

Typically a good-performance brain PET imager is heavy and not motion-tolerant. It requires the patient to lay still in a supine or prone position, like in the MRI case. A high-sensitivity imager is typically more heavy and bulky and wearing it with or without mechanical support presents higher safety hazard. High time resolution performing TOF capable electronics is complicated, even more bulky and heavy, with increased cable burden and typically generates more heat requiring active cooling, etc. However, the key limiting factor is the stopping power of the radiation sensor dependent on the amount and weight of the heavy scintillator material. Any wearable scheme must recognize this fact and the imposed limitations. Unlike in cancer diagnostics, lower sensitivity (translating into higher injected imaging agent dose and/or poorer event statistics) creates a barrier to many applications where radiation dose is an issue, such as brain research in healthy

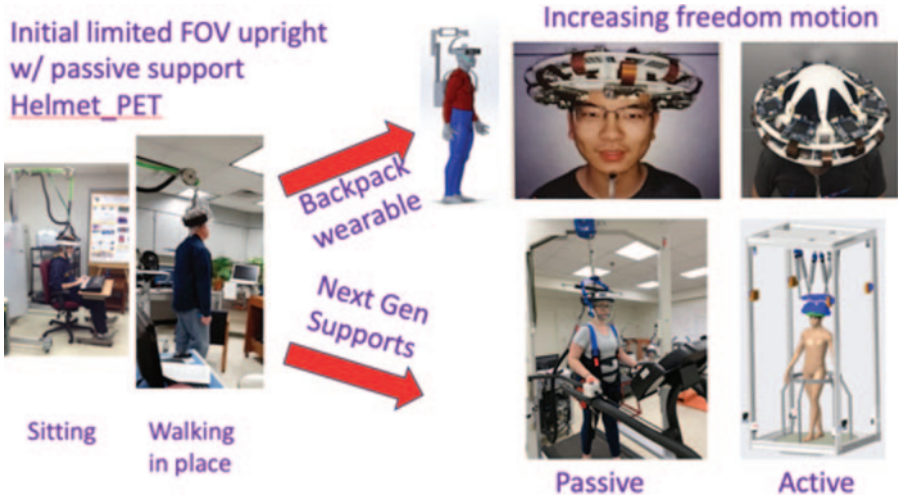

Fig. 28. – Two separate trajectories of development of the motion-tolerant upright imagers. A wearable backpack-supported system provides maximum motion tolerance at the expense of sensitivity Implementation of intelligent robotic supports may indeed solve the issue of the limited axial coverage and poor sensitivity of the first generation of wearable brain PET systems. (Left and passive bottom pictures are from the WVU ring project, kindly provided by Julie Brefczynski-Lewis. Top right: MindTracker [16], kindly provided by Qiyu Peng, Berkeley. Sketch at the bottom right kindly provided by Peter Kazanzides from JHU).

subjects but also screening tests for many conditions, such as dementia, depression, mTBI in sports, stroke, etc.

Therefore, the key challenge that one is facing is how to balance between the sensitivity and brain coverage (=weight) and the motion tolerance of the overall system, and how swiftly and safely mechanical support can follow the moving head in 3D. The integral part of the imager system will be the motion correction system that at all times records and provides the reconstruction software with the absolute and relative positions of the head and of the imager's sensor/gamma detector.

Indeed, at the heart of such development efforts is the quest of how to maximize in a safe way the motion tolerance for the subject's head and torso/body movements using the latest technological developments in motion correction, both hardware and software. Part of the discussed cutting-edge approach is predicting the subject intentions and promptly responding, but again with patient comfort and safety having the highest priority. This is the main challenge that needs to be resolved.

One theoretically considered approach to the weight issue is not only to improve the intelligent mechanical support, but also to decrease the amount of (heavy and expensive) scintillator, while maintaining the same sensitivity performance. The estimates of the TOF-delivered boost to the sensitivity and S/N at 30–50 ps FWHM CRT stipulate that the amount of LSO/LYSO can be decreased by 60–70% with substantial weight savings.

Potentially the best practical solution to this basic conflict between sensitivity and motion tolerance is to develop a system that will recreate realistic environment using high-performance detectors placed close to the head but not touching the head. The critical part of this approach is the concept of "compressing" the physical world and creating a close to realistic environment approximation or simulation of the real-world experience in the laboratory by a combination of advanced mechanical and software

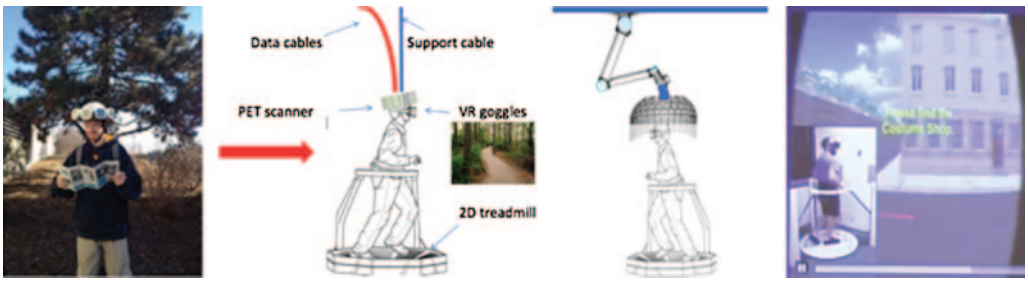

Fig. 29. – Application of the concept of "compressing the world" to upright PET brain imaging. The real world was here compressed to a small size. The subject is immersed in the VR world. The imaging brain with PET imager during the "walk in the park" experience using a wearable backpack-supported system (left) is recreated in the laboratory using the 2D 360° treadmill which allows for walking forward, turning, going backwards and even running. The subject is secured by a barrier. On the right we shown an example frame from a navigational test using VR goggles and treadmill in Arne Ekstrom's lab at UC Davis. These types of studies allow "studying large scale (∼1 km) spatial navigation in free ambulating room". (`https://www.youtube.com/watch?v=xug0ffORsgY`). Ideally, the VR/AR goggles should be comfortable, occupy little space, be lightweight, provide little burden to the subject/patient and most importantly NOT conflict with the PET scanner and other sensors. The concept at center-left has a supported wearable imager, and the one at center-right is a dome-type imager supported by a robotic arm attached to the ceiling, in this case.

measures. Using VR or AR including video and audio and potentially other effects will create this "compressed world". In fact, VR/AR has the important advantage of creating a controlled and reproducible environment, which is mostly not feasible in the real world. Importantly, this "space compression" greatly facilitates solutions to the challenge imposed by the safe and functional mechanical support issues and indeed allows implementation of heavier and more bulky detectors with high sensitivity, the solution that would be prohibitive in the real "walk in the park" implementation, for example when using a backpack-supported system. In addition, application of compact VR goggles can permit better angular head (and brain) coverage while making the experience more comfortable for the subjects/patients.

10. – Conclusions

The modern compact MRI-compatible SiPM technology with constantly improving TOF performance allows one to design a variety of dedicated brain imaging PET structures that can cover the full range of applications, including mobile systems. Potentially the main impact is expected on the sensitivity of the detector, and following the example of the total-body Explorer PET scanner, high-quality kinetic brain studies will become possible with powerful parametric imaging. TOF CTR performance at the level of 30–50 ps FWHM may become available in a few years and provide further boost to the sensitivity of the scanner.

* * *

I thank my new friend Angelo Pagano who, inspired by my old friend Franco Garibaldi, invited me to give this talk at the FATA meeting and for the extremely friendly hospitality during the conference, assisted by his equally friendly team of helpers. But primarily I thank and congratulate him again for his bright vision and persistence to organize

this extremely useful thematic conference. And for deciding with the help of Sara Pirrone and others to produce this conference record. Many people contributed to the pool of information from which the (necessary) selection was made for this report, due to space limitation, and their incomplete list with unintended unfortunate omissions (for which I profusely apologize) is included here: Ramsey Badawi, Nicola Belcari, Jose Maria Bennloch, Giacomo Borghi, Julie Brefczynski-Lewis, Richard Carson, Cyprian Catana, Simon Cherry, Seng Choong, Junwei Du, Gerard Ariño Estrada, George El Fakhri, Giovanni Frizoni, Franco Garibaldi, Andrew Goertzen, Alberto Gola, Antonio Gonzalez, William Jagust, Terry Jones, Peter Kazanzides, Paul Kinahan, Peter Krizan, Andrzej Krol, Bijoy Kundu, Sandi Kwee, Sun Il Kwon, Karol Lang, Paul Lecoq, Jae-Sung Lee, Elizabeth Li, Hongdi Li, Michael Minot, Robert Miyaoka, Johan Nuyts, Caroline Paquette, Qiyu Peng, Rok Pestotnik, John Prior, Jinyi Qi, Arman Rahmim, Hamid Sabet, Jeff Schmall, Ross Schmidtlein, Paul Schotanus, Youngho Seo, Alexander Stolin, Yuan-Chuan Tai, Stefaan Tavernier, Charalampos (Harry) Tsoumpas, Stefaan Vanderberghe, William Worstell, Qingguo Xie, Seiichi Yamamoto, Taiga Yamaya, Xuezhu Zhang, and others.

REFERENCES

[1] Yamaya T., Yoshida E., Obi T., Ito H., Yoshikawa K. and Murayama H., *IEEE Trans. Nucl. Sci.*, **55** (2008) 2482.

[2] González Antonio J., Majewski Stan, Sánchez Filomeno, Aussenhofer Sebastian, Aguilar Albert, Conde Pablo, Hernández Liczandro, Vidal Luis F., Pani Roberto, Bettiol Marco, Fabbri Andrea, Bert Julien, Visvikis Dimitris, Jackson Carl, Murphy John, O'Neill Kevin and Benlloch Jose M., *Nucl. Instrum. Methods Phys. Res. A*, **818** (2016) 82.

[3] Grogg K. S., Toole T., Ouyang J., Zhu X., Normandin M. D., Li Q., Johnson K., Alpert N. M. and El Fakhri G., *J. Nucl. Med.*, **57** (2016) 646.

[4] HitPET-Hamamatsu, Hamamatsu Photonics K. K., Hamamatsu City, Japan.

[5] Watanabe M., Saito A., Isobe T., Ote K., Yamada R., Moriya T. and Omura T., *Phys. Med. Biol.*, **62** (2017) 7148.

[6] Gómez Herrero Juan A., García José Navarro, Atienza Vicente Carlos M., Peris Serra José L., Solera Navarro María Jesús, Mascarell Juan Catret and Benlloch Babiera José María, *Development of a new device for the early diagnosis of Alzheimer's disease. Rev. Biomech.*, `http://www.biomecanicamente.org/item/1159-rb65-caremibrain-english.html?tmpl=component&print=1`.

[7] CareMiBrain imager, ONCOVISION, Valencia, Spain, `https://www.oncovision.com`.

[8] Benlloch José M., González Antonio J., Pani Roberto, Preziosi Enrico, Jackson Carl, Murphy John, Barberá Julio, Correcher Carlos, Aussenhofer Sebastian, Gareis Daniel, Visvikis Dimitris, Bert Julien, Langstrom Bengt, Farde Lars, Toth Miklos, Haggkvist Jenny, Caixeta Fabio V., Kullander Klas, Somlai-Schweiger Ian and Schwaiger Markus, *Eur. Psychiatry*, **50** (2018) 21.

[9] Majewski S. and Proffitt J., *Compact and mobile high resolution PET brain imager*, US Patent. 7,884,331 (2011).

[10] Majewski S., Proffitt J., Brefczynski-Lewis J., Stolin A., Weisenberger A. G., Xi W. and Wojcik R., *HelmetPET: A silicon photomultiplier based wearable brain imager,* in *Proceedings of the IEEE Nuclear Science Symposium and Medical Imaging Conference Record, Valencia, Spain, 23–29 October 2011* (IEEE) 2012, pp. 4030–4034.

[11] Bauer C. E., Brefczynski-Lewis J., Marano G., Mandich, M.-B., Stolin A., Martone P., Lewis J. W., Jaliparthi G., Raylman R. R. and Majewski S., *Brain Behav.*, **6** (2016) e00530.

[12] Melroy S., Bauer C., McHugh M., Carden G., Stolin A., Majewski S., Brefczynski-Lewis J. and Wuest T., *Sensors*, **17** (2017) 1164.
[13] Majewski S. and Brefczynski-Lewis J., *VIRPET–Combination of Virtual Reality and PET Brain Imaging*, US Patent 9,655,573 (2017).
[14] Yamamoto S., Honda M., Shimizu K. and Senda M., *J. Nucl. Med.*, **50** (2009) 1532.
[15] Yamamoto S., Honda M., Oohashi T., Shimizu K. and Senda M., *IEEE Trans. Nucl. Sci.*, **58** (2011) 668.
[16] Xu Jianfeng, Zhao Zhixiang, Xie Siwei, Shi Dawei, Huang Qiu and Peng Qiyu, *Mind-Tracker PET: A wearable PET camera for brain imaging,* in *Proceedings of the IEEE Nuclear Science Symposium and Medical Imaging Conference Record, Atlanta, Georgia, USA, 21–28 October 2017* (IEEE) 2018.
[17] Phelps M. E., *J. Nucl. Med.*, **41** (2000) 661.
[18] BRAIN_Working_Group, *BRAIN 2025 report*, available from: `https://braininitiative.nih.gov/strategic-planning/brain-2025-report`.
[19] Laruelle M., *J. Cereb. Blood Flow Metab.*, **20** (2000) 423.
[20] Fung E. K. and Carson R. E., *Phys. Med. Biol.*, **58** (2013) 1903.
[21] Faul M. and Coronado V., *Epidemiology of traumatic brain injury,* in *Handbook of Clinical Neurology*, Vol. **127** (Elsevier) 2015, pp. 3–13.
[22] Morbelli S., Garibotto V., Van De Giessen E., Arbizu J., Chetelat G., Drezgza A., Hesse S., Lammertsma A. A., Law I., Pappata S., Payoux P. and Pagani M., *Eur. J. Nucl. Med. Mol. Imaging*, **42** (2015) 1487.
[23] Finnema S. J., Nabulsi N. B., Eid T., Detyniecki K., Lin S. F., Chen M. K., Dhaher R., Matuskey D., Baum E., Holden D., Spencer D. D., Mercier J., Hannestad J., Huang Y. and Carson R. E., *Sci. Transl. Med.*, **8** (2016) 348ra96.
[24] Kelley P., Evans M. D. R. and Kelley J., *Front. Hum. Neurosci.*, **12** (2018) 400.
[25] Chen M. K., Mecca A. P., Naganawa M., Finnema S. J., Toyonaga T., Lin S. F., Najafzadeh S., Ropchan J., Lu Y., McDonald J. W., Michalak H. R., Nabulsi N. B., Arnsten A. F. T., Huang Y., Carson R. E. and van Dyck C. H., *JAMA Neurol.*, **75** (2018) 1215.
[26] Carson R. E. and Kuo P. H., *IEEE Trans. Radiat. Plasma Med. Sci.*, **3** (2019) 254.
[27] Hooker J. M. and Carson R. E., *Annu. Rev. Biomed. Eng.*, **21** (2019) 551.
[28] Funck T., Palomero-Gallagher N., Omidyeganeh M., Lepage C., Toussaint P. J., Khalili N., Zilles K., Evans A. C. and Thiel A., *J. Cereb. Blood Flow Metab.*, **39(1 Suppl.)** (2019) 1, BPS04-6.
[29] Molnar Z., Clowry G. J., Sestan N., Alzu'bi A., Bakken T., Hevner R. F., Huppi P. S., Kostovic I., Rakic P., Anton E. S., Edwards D., Garcez P., Hoerder-Suabedissen A. and Kriegstein A., *J. Anat.*, **235** (2019) 432.
[30] The Siemens Biograph Vision PET/CT, `https://www.siemens-healthineers.com/en-us/molecular-imaging/pet-ct/biograph-vision`.
[31] van Sluis J., de Jong J., Schaar J., Noordzij W., van Snick P., Dierckx R., Borra R., Willemsen A. and Boellaard R., *J. Nucl. Med.*, **60** (2019) 1031.
[32] Wienhard K., Schmand M., Casey M., Baker K., Bao J., Eriksson L., Jones W., Knoess C., Lenox M. and Lercher M., *IEEE Trans. Nucl. Sci.*, **49** (2002) 104.
[33] Eriksson L., Wienhard K., Eriksson M. *et al.*, *IEEE Trans. Nucl. Sci.*, **49** (2002) 2085.
[34] VanVelden F. H., Kloet R. W., van Berckel B. N., Buijs F. L., Luurtsema G., Lammertsma A. A. and Boellaard R., *J. Nucl. Med.*, **50** (2009) 693.
[35] Olesen O. V., Sibomana M., Keller S. H., Anderson F., Jensen J., Holm S. and Hjgaard L., *Spatial resolution of the HRRT PET scanner using 3D-OSEM PSF reconstruction,* in *IEEE Nuclear Science Symposium Conference Record* (IEEE) 2009, pp. 3789–3790.
[36] Tashima H. and Yamaya T., *Phys. Med. Biol.*, **61** (2016) 7205.
[37] Ahmed A. M., Tashima H., Yoshida E., Nishikido F. and Yamaya T., *Phys. Med. Biol.*, **62** (2017) 4541.

[38] Ahmed A. M., Tashima H., Yoshida E. and Yamaya T., *Nucl. Instrum. Methods Phys. Res. A*, **858** (2017) 96.
[39] González Antonio J., Sánchez Filomeno, Conde Pablo, Aussenhofer Sebastian, Gareis Daniel, Pani Roberto, Pellegrini Rossana, Bettiol Marco, Fabbri Andrea, Majewski Stan, Bauer Christian, Stolin Alexander, Martone Peter, Bert Julien, Visvikis Dimitris, Jackson Carl, Murphy John, O'Neill Kevin and Benlloch Jose M., *A novel brain PET insert for the MINDView project,* in *IEEE NSS-MIC Conference Record (Seattle, US)* (IEEE) 2014.
[40] Pani R., Gonzalez A. J., Bettiol M., Fabbri A., Cinti M. N., Preziosi E., Borrazzo C., Conde P., Pellegrini R., Di Castro E. and Majewski S., *J. Instrum.*, **10** (2015) C06006.
[41] Lyu Y., Lv X., Liu W., Judenhofer M. S., Zwingenberger A., Wisner E. R., Berg E., McKenney S. E., Leung E. K. and Spencer B. A., *Phys. Med. Biol.*, **64** (2019) 075004.
[42] Lee Jae Sung, *Open Nucl. Med. J.*, **2** (2010) 192.
[43] Kolb A., Wehrl H. F., Hofmann M., Judenhofer M. S., Eriksson L., Ladebeck R., Lichy M. P., Byars L., Michel C. and Schlemmer, H.-P., *Eur. Radiol.*, **22** (2012) 1776.
[44] González A. J., Conde P., Hernández L., Herrero V., Moliner L., Monzó J. M., Orero A., Peiró A., Rodríguez-Álvarez M. J., Ros A., Sánchez F., Soriano A., Vidal L. F. and Benlloch J. M., *Nucl. Instrum. Methods A*, **702** (2013) 94.
[45] Bauer C., Stolin A., Proffitt J., Martone P., Brefczynski-Lewis J. A., Lewis J. W., Hankiewicz J., Raylman R. and Majewski S., *Development of a ring PET insert for MRI,* in *IEEE Nuclear Science Symposium and Medical Imaging Conference* (IEEE) 2013, pp. 1–9.
[46] Cho Gyuseng, Choi Yong, Lee Jae Sung, An Hyun Joon, Jung Jin Ho, Park Hyun Wook, Oh Chang Hyun, Park Kyeongjin, Lim Kyung Taek, Cho Minsik, Sul Woo Suk, Kim Hyoungtaek and Kim Hyunduk, *EJNMMI Phys.*, **1(Suppl 1)** (2014) A13.
[47] Chen S., Cao T., Dong Y., Liu S., Yang G., Zhao Y., Chen X., Hu L. and Shi H., *J. Nucl. Med.*, **59(supplement 1)** (2018) 215.
[48] González Antonio J., Majewski Stan, Sánchez Filomeno, Aussenhofer Sebastian, Aguilar Albert, Conde Pablo, Hernández Liczandro, Vidal Luis F., Pani Roberto, Bettiol Marco, Fabbri Andrea, Bert Julien, Visvikis Dimitris, Jackson Carl, Murphy John, O'Neill Kevin and Benlloch Jose M., *Nucl. Instrum. Methods Phys. Res. A*, **818** (2016) 82.
[49] Cal-Gonzalez Jacobo, Rausch Ivo, Sundar Lalith K. Shiyam, Lassen Martin L., Muzik Otto, Moser Ewald, Papp Laszlo and Beyer Thomas, *Front. Phys.*, **6** (2018) 47.
[50] Chen S., Hu P., Gu Y., Pang L., Zhang Z., Zhang Y., Meng X., Cao T., Liu X. and Fan Z., *J. Appl. Clin. Med. Phys.*, **20** (2019) 184.
[51] Hoffman E. J., Huang S. C. and Phelps M. E., *J. Comput. Assist. Tomogr.*, **3** (1979) 299.
[52] Wahl R. L., *Principles and Practice of PET and PET/CT*, 2nd edition (Lippincott Williams & Wilkins, Philadelphia, PA) 2008.
[53] Lewellen T. K., *Phys. Med. Biol.*, **53** (2008) R287.
[54] Lewellen T. K., *Am. J. Roentgenol.*, **195** (2010) 301.
[55] Peng Hao and Levin Craig S., *Curr. Pharm. Biotechnol.*, **11** (2010) 555.
[56] Lee Jae Sung, *Open Nucl. Med. J.*, **2** (2010) 192.
[57] Vaquero J. J. and Kinahan P., *Annu. Rev. Biomed. Eng.*, **17** (2015) 385.
[58] Del Guerra A., Belcari N. and Bisogni M., *Riv. Nuovo Cimento*, **39** (2016) 155.
[59] Walrand S., Hesse M. and Jamar F., *Br. J. Radiol.*, **89** (2018) 20160534.
[60] Jones T. and Townsend D., *J. Med. Imaging*, **4** (2017) 011013.
[61] Berg Eric and Cherry Simon R., *Semin. Nucl. Med.*, **48** (2018) 311.

[62] Anishchenko Sergey, Beylin David, Stepanov Pavel, Stepanov Alex, Weinberg Irving N., Schaeffer Stephen, Zavarzin Valery, Shaposhnikov Dmitry and Smith Mark F., *Markerless head tracking evaluation with human subjects for a dedicated brain PET scanner,* in *IEEE Nuclear Science Symposium and Medical Imaging Conference (NSS/MIC)* (IEEE) 2015.
[63] Anishchenko S., Beylin D., Stepanov P., Stepanov A., Weinberg I. N., Schaeffer S., Zavarzin V., Shaposhnikov D. and Smith M. F., *Proc. SPIE*, **9412** (2015) 94121P.
[64] Beylin D., Anishchenko S., Smith M. F., Stepanov P., Stepanov A., Zavarzin V., Schaeffer S. and Weinberg, I. N., *Medical imaging systems and methods for performing motion-corrected image reconstruction* US Patent. 20160247293 A1 (2016).
[65] Miyaoka R. S., Lewellen T. K., Yu H. and McDaniel D. L., *IEEE Trans. Nucl. Sci.*, **45** (1998) 1069.
[66] Virador P. R. G. *et al.*, *IEEE Trans. Nucl. Sci.*, **48** (2001) 1524.
[67] Liu H., Omura T., Watanabe M. and Yamashita T., *Nucl. Instrum. Methods Phys. Res. A*, **459** (2001) 182.
[68] Yang Y., Dokhale P. A., Silverman R. W. *et al.*, *Phys. Med. Biol.*, **51** (2006) 2131.
[69] Yang Y., Wu Y. B., Qi J. *et al.*, *J. Nucl. Med.*, **49** (2008) 1132.
[70] Trummer J., Auffray E. and Lecoq P., *Nucl. Instrum. Methods Phys. Res. A*, **599** (2009) 264.
[71] Yang Y., Wu Y. and Cherry S. R., *IEEE Trans. Nucl. Sci.*, **56** (2009) 2594.
[72] St James S., Yang Y. F., Wu Y. B. *et al.*, *Phys. Med. Biol.*, **54** (2009) 4605.
[73] Ito M., Lee J. S., Kwon S. I., Lee G. S., Hong B., Lee K. S., Sim K. S., Lee S. J., Rhee J. T. and Hong S. J., *IEEE Trans. Nucl. Sci.*, **57** (2010) 976.
[74] Yang Y., St James S., Wu Y. B. *et al.*, *Phys. Med. Biol.*, **56** (2011) 139.
[75] Ito M., Hong S. J. and Lee J. S., *Biomed. Eng. Lett.*, **1** (2011) 70.
[76] Ito M., Lee M. S. and Lee J. S., *Phys. Med. Biol.*, **58** (2013) 1269.
[77] Wiener R., Surti S. and Karp J., *IEEE Trans. Nucl. Sci.*, **60** (2013) 1478.
[78] Brown M. S., Gundacker S., Taylor A., Tummeltshammer C., Auffray E., Lecoq P. and Papakonstantinou I., *PLOS ONE*, **9** (2014) 1.
[79] Shao Y., Sun X., Lan K. A., Bircher C., Lou K. and Deng Z., *Phys. Med. Biol.*, **59** (2014) 1223.
[80] Matsumoto T., Yamaya T., Yoshida E., Nishikido F., Inadama N., Murayama H. and Sug M., *Radiol. Phys. Technol.*, **7** (2014) 43.
[81] Kolb A., Parl C., Mantlik F., Liu C. C., Lorenz E., Renker D. and Pichler B. J., *Med. Phys.*, **41** (2014) 081916.
[82] Schmall J. P., Surti S. and Karp J. S., *Phys. Med. Biol.*, **60** (2015) 3549.
[83] Kang H. G., Ko G. B., Rhee J. T., Kim K. M., Lee J. S. and Hong S., *IEEE Trans. Nucl. Sci.*, **62** (2015) 1935.
[84] Pizzichemi M., Stringhini G., Niknejad T., Liu Z., Lecoq P., Tavernier S., Varela J., Paganoni M. and Auffray E., *Phys. Med. Biol.*, **61** (2016) 4679.
[85] Pani Roberto, Bettiol Marco, Preziosi Enrico, Borrazzo Cristian, Pellegrini Rosanna, González Antonio J., Conde Pablo, Cinti Maria Nerina, Fabbri Andrea, Di Castro Elisabetta and Majewski Stan, *Trans. Nucl. Sci.*, **63** (2016) 2487.
[86] Schmall J. P., Karp J. S., Werner M. and Surti S., *Phys. Med. Biol.*, **61** (2016) 5443.
[87] Marcinkowski Radoslaw, Mollet Pieter, Van Holen Roel *et al.*, *Phys. Med. Biol.*, **61** (2016) 2196.
[88] Niknejad T., Pizzichemi M., Stringhini G., Auffray E., Bugalho R., Silva J. C. D., Francesco A. D., Ferramacho L., Lecoq P., Leong C., Paganoni M., Rolo M., Silva R., Silveira M., Tavernier S., Varela J. and Zorraquino C., *Nucl. Instrum. Methods Phys. Res. Sect. A*, **845** (2017) 684.
[89] Du J., Bai X., Gola A., Acerbi F., Ferri A., Piemonte C., Yang Y. and Cherry S. R., *Phys. Med. Biol.*, **63** (2018) 035035.

[90] Nitta Munetaka, Inadama Naoko, Nishikido Fumihiko, Yoshida Eiji, Tashima Hideaki, Kawai Hideyuki and Yamaya Taiga, *IEEE Trans. Radiat. Plasma Med. Sci.*, **2** (2018) 564.
[91] Du J., Bai X. and Cherry S. R., *Phys. Med. Biol.*, **64** (2019) 15NT03.
[92] Han Young Been, Kang Han Gyu, Song Seong Hyun, Ko Guen Bae, Lee Jae Sung and Hong Seong Jong, *J. Instrum.*, **14** (2019) P02023.
[93] Du Junwei, Bai Xiaowei and Cherry Simon R., *Phys. Med. Biol.*, **64** (2019) 15NT03.
[94] Lopresti B. J., Russo A. *et al.*, *IEEE Trans. Nucl. Sci.*, **46** (1999) 2059.
[95] Teimoorisichani Mohammadreza and Goertzen Andrew L., *Phys. Med. Biol.*, **64** (2019) 115007.
[96] Shao Y., Cherry S. R., Siegel S. and Silverman R. W., *IEEE Trans. Nucl. Sci.*, **43** (1996) 1938.
[97] Stickel J. R. and Cherry S. R., *Phys. Med. Biol.*, **50** (2005) 179.
[98] Yang Y., Dokhale P. A., Silverman R. W., Shah K. S., McClish M. A., Farrell R., Entine G. and Cherry S. R., *Phys. Med. Biol.*, **51** (2006) 2131.
[99] Lodge M. A., Rahmim A. and Wahl R. L., *J. Nucl. Med.*, **50** (2009) 1307.
[100] Moses W. W., *Nucl. Instrum. Methods Phys. Res. A*, **648(supplement 1)** (2011) S236.
[101] Yamamoto S., Watabe H., Kanai Y., Watabe T., Kato K. and Hatazawa J., *Phys. Med. Biol.*, **58** (2013) 7875.
[102] Rodríguez-Villafuerte M., Yang Y. and Cherry S., *Phys. Med.*, **30** (2014) 76.
[103] Yin Y. Z., Chen X. M., Li C. Z., Wu H. Y., Komarov S., Guo Q. Z., Krawczynski H., Meng L. J. and Tai Y. C., *IEEE Trans. Nucl. Sci.*, **61** (2014) 154.
[104] España S., Marcinkowski R., Keereman V., Vandenberghe S. and Van Holen R., *Phys. Med. Biol.*, **59** (2014) 3405.
[105] Wang Q., Wen J., Ravindranath B., O'Sullivan A. W., Catherall D., Li K., Wei S., Komarov S. and Tai Y. C., *Nucl. Instrum. Methods Phys. Res. A.*, **794** (2015) 151.
[106] Yang Yongfeng, Bec Julien, Zhou Jian, Zhang Mengxi, Judenhofer Martin S., Bai Xiaowei, Di Kun, Wu Yibao, Rodriguez Mercedes, Dokhale Purushottam, Shah Kanai S., Farrell Richard, Qi Jinyi and Cherry Simon R., *J. Nucl. Med.*, **57** (2016) 1130.
[107] Gong K., Cherry S. R. and Qi J., *Phys. Med. Biol.*, **61** (2016) N193.
[108] Marcinkowski Radoslaw, Mollet Pieter, Van Holen Roel *et al.*, *Phys. Med. Biol.*, **61** (2016) 2196.
[109] Mollet Pieter, Deprez Karel, Vandeghinste Bert, Neyt Sara, Marcinkowski Radoslaw, Vandenberghe Stefaan and Van Holen Roel, *J. Nucl. Med.*, **58(supplement 1)** (2017) 393.
[110] Emilie Gaudin *et al.*, *Imaging performance of a submillimetric spatial resolution APD-based preclinical PET scanner dedicated to mouse imaging*, presented at the IEEE MIC, Atlanta, 21–28 October 2017.
[111] Godinez Felipe, Gong Kuang, Zhou Jian, Judenhofer Martin S., Chaudhari Abhijit J. and Badawi Ramsey D., *IEEE Trans. Radiat. Plasma Med. Sci.*, **2** (2018) 7.
[112] Du Junwei, Bai Xiaowei and Cherry Simon, *Design and development of detector modules for high-resolution and high-sensitivity brain PET*, presented at the IEEE MIC, Atlanta, 21–28 October 2017.
[113] Du Junwei, Bai Xiaowei, Liu Chih-Chieh, Qi Jinyi and Cherry Simon R., *Phys. Med. Biol.*, **64** (2019) 235004.
[114] Szanda I., Mackewn J., Patay G. *et al.*, *J. Nucl. Med.*, **52** (2011) 1741.
[115] NEMA Standards Publication NU 4-2008, *Performance measurements of small animal positron emission tomography*, (National Electrical Manufacturers Association, Rosslyn, VA) 2008.

[116] Rahmim A., Lodge M. A., Crabb A. H., Zhou Y., Wong D. F. and Gottesman R. F., *Simultaneous monitoring of PET image resolution, noise, uniformity and quantitative accuracy using uniform cylinder phantom measurements in the multi-center setting,* in *2014 IEEE Nuclear Science Symposium and Medical Imaging Conference (NSS/MIC)* (IEEE) 2014.
[117] Sabbir Ahmed S. M., Demir Mustafa, Kabasakal Levent and Uslu Ilhami, *Med. Phys.*, **32** (2005) 530.
[118] Chiang Fu-Tsai, Li Pei-Jung, Chung Shih-Ping, Pan Lung-Fa and Pan Lung-Kwang, *Bioengineered*, **7** (2016) 304.
[119] Rausch I., Ruiz A., Valverde-Pascual I., Cal-González J., Beyer T. and Carrio I., *J. Nucl. Med.*, **60** (2019) 561.
[120] Daube-Witherspoon M., Yan Y., Green M., Carson R., Kempner K. and Herscovitch P., *J. Nucl. Med.*, **31** (1990) 816.
[121] Fulton R. R., Meikle S. R., Eberl S., Pfeiffer J., Constable C. J. and Fulham M. J., *IEEE Trans. Nucl. Sci.*, **49** (2002) 116.
[122] Carson R. E., Barker W. C., Liow J.-S., Adler S. and Johnson C. A., *Design of a motion-compensation OSEM list-mode algorithm for resolution-recovery reconstruction of the HRRT,* in *IEEE Nuclear Science Symposium and Medical Imaging Conference, Portland, OR* (IEEE) 2003.
[123] Bloomfield P. M., Spinks T. J., Reed J., Schnorr L., Westrip A. M., Livieratos L., Jones T. *et al.*, *Phys. Med. Biol.*, **48** (2003) 959.
[124] Bloomfield P. M., Spinks T. J., Reed J., Schnorr L., Westrip A. M., Livieratos L., Fulton R. and Jones T., *Phys. Med. Biol.*, **48** (2003) 959.
[125] Rahmim A., Rousset O. G. and Zaidi H., *PET Clinics*, **2** (2007) 251.
[126] Rahmim A., Dinelle K., Cheng J. C., Shilov M. A., Segars W. P., Lidstone S. C., Blinder S., Rousset O. G., Vajihollahi H., Tsui B. M. W., Wong D. F. and Sossi V., *IEEE Trans. Med. Imaging*, **27** (2008) 1018.
[127] Rahmim A., Cheng J. C., Dinelle K., Shilov M., Segars W. P., Rousset O. G., Sossi V. *et al.*, *Nucl. Med. Commun.*, **29** (2008) 574.
[128] Rahmim A., Tang J. and Zaidi H., *Med. Phys.*, **36** (2009) 3654.
[129] Rahmim A., Tang J., Ay M. R. and Bengel F., *4D respiratory motion-corrected Rb-82 myocardial perfusion PET imaging,* in *IEEE Nuclear Science Symposium Conference Record* (IEEE) 2010, pp. 3312–3316.
[130] Keller S. H., Sibomana M., Olesen O. V., Svarer C., Holm S., Andersen F. L. and Højgaard L., *J. Nucl. Med.*, **53** (2012) 495.
[131] Jin X., Mulnix T., Gallezot J. D. and Carson R. E., *Med. Phys.*, **40** (2013) 102503.
[132] Rahmim A., Tang J. and Zaidi H., *PET Clinics*, **8** (2013) 51.
[133] Olesen O. V., Sullivan J. M., Mulnix T., Paulsen R. R., Hojgaard L., Roed B., Carson R. E., Morris E. D. and Larsen R., *IEEE Trans. Med. Imaging*, **32** (2013) 200.
[134] Noonan P. J., Howard J., Hallett W. A. and Gunn R. N., *Phys. Med. Biol.*, **60** (2015) 8753.
[135] Mohy-ud-Din H., Nicolas A., Willis W., Abdel K., Dean F. and Rahmim A., *Front. Biomed. Technol.*, **2** (2015) 366.
[136] Pohlmann S. T., Harkness E. F., Taylor C. J. and Astley S. M., *J. Med. Biol. Eng.*, **36** (2016) 857.
[137] Ren S., Jin X., Chan C., Jian Y., Mulnix T., Liu C. and Carson R. E., *Phys. Med. Biol.*, **62** (2017) 4741.
[138] Kim S. and Kazanzides P., *Int. J. Comput. Assist. Radiol. Surg.*, **12** (2017) 277.
[139] Wang J., Qian L., Azimi E. and Kazanzides P., *Prioritization and static error compensation for multi-camera collaborative tracking in augmented reality,* in *IEEE Virtual Reality, Los Angeles, CA* (IEEE) 2017, pp. 335–336.
[140] Kyme A. Z., Se S., Meikle S. R. and Fulton R. R., *Phys. Med. Biol.*, **63** (2018) 105018.

[141] Lu Y., Gallezot J. D., Naganawa M., Fontaine K., Toyonaga T., Ren S., Mulnix T., Liu C. and Carson R., *J. Nucl. Med.*, **59(supplement 1)** (2018) 98.

[142] Lu Y., Gallezot J. D., Naganawa M., Ren S., Fontaine K., Wu J., Onofrey J. A., Toyonaga T., Boutagy N., Mulnix T., Panin V. Y., Casey M. E., Carson R. E. and Liu C., *Phys. Med. Biol.*, **64** (2019) 065002.

[143] Ren S., Lu Y., Bertolli O., Thielemans K. and Carson R. E., *Phys. Med. Biol.*, **64** (2019) 165014.

[144] Sun C., Fontaine K., Revilla E., Toyonaga T., Gallezot J. D., Mulnix T., Carson R. and Lu Y., *A data-driven quality control method for head motion tracking in PET,* in *IEEE NSS/MIC* (IEEE) 2019.

[145] Hurley S., Spangler-Bickell M., Deller T., Bradshaw T., Jansen F. and McMillan A., *J. Nucl. Med.*, **60(supplement 1)** (2019) 1358.

[146] Berker Yannick, Schulz Volkmar and Karp Joel S., *EJNMMI Phys.*, **6** (2019) 18.

[147] Harrison R. L., Elston B. F., Majewski S., Qi J., Manjeshwar R., Dolinsky S. Kinahan P. E. *et al.*, *Sensitivity analysis for the design of a wearable PET brain scanner*, IEEE MIC Poster Presentation, San Diego, CA (2015).

[148] Gong K., Majewski S., Kinahan P. E., Harrison R. L., Elston B. F., Manjeshwar R., Dolinsky S., Stolin A. V., Brefczynski-Lewis J. A. and Qi J., *Phys. Med. Biol.*, **61** (2016) 3681.

[149] Shin Han-Back, Choi Yong, Huh Yoonsuk, Jung Jin Ho and Suh Tae Suk, *Prog. Med. Phys.*, **27** (2016) 236.

[150] Schmidtlein C. R. *et al.*, *Proc. SPIE*, **9788** (2016) 978806.

[151] Schmidtlein C. R., Turner J. N., Thompson M. O., Mandal K. C., Haggstrom Zhang J., Humm J. L., Feiglin D. H. and Krol A., *J. Med. Imaging*, **4** (2017) 011003.

[152] Shi H., Du D., Xu J. and Peng Q., *Assessment of dedicated brain PET designs with different geometries,* in *IEEE MIC* (IEEE) 2013.

[153] Shi H., Du D., Xu J. and Peng Q., *PMT based pentagonal and hexagonal detector module designs for convex polyhedron PET systems,* in *IEEE MIC* (IEEE) 2013.

[154] Shi Han, Du Dong, Xu JianFeng, Su Zhihong and Peng Qiyu, *Technol. Health Care*, **23** (2015) S615.

[155] Xu JianFeng, Huang Qiu, Weng Fenghua, Zan Yunlong, Chen Jie, Xie Siwei, Zhao Zhixiang, Li Hongyuan, Tao Weijie, Zhu Yicheng and Peng qiyu, *Progresses in designing a high-sensitivity dodecahedral PET for brain imaging,* in *Nuclear Science Symposium, Medical Imaging Conference and Room-Temperature Semiconductor Detector Workshop (NSS/MIC/RTSD)* 2016, https://doi.org/10.1109/NSSMIC.2016.8069608.

[156] Gaudin Emilie, Toussaint Maxime, Thibaudeau Christian, Paille Maxine, Fontaine Rejean and Lecomte Roger, *IEEE Trans. Radiat. Plasma Med. Sci.*, **3** (2019) 334.

[157] Catana Ciprian, *J. Nucl. Med.*, **60** (2019) 1044.

[158] Vinke R. and Levin C. S., *Phys. Med. Biol.*, **59** (2014) 2975.

[159] Benlloch J. M., Carrilero V., González A., Catret J. J., Lerche Ch. W., Abellán D., García de Quirós F., Giménez M., Modia J., Sánchez F., Pavón N., Rosa A., Martínez J. and Sebastiá A., *Nucl. Instrum. Methods A*, **571** (2007) 26.

[160] Miyaoka R. S., Li X. L., Lockhart C. and Lewellen T. K., *Design of a high resolution, monolithic crystal PET/MRI detector with DOI positioning capability,* in *IEEE Nuclear Science Symposium Conference Record* (IEEE) 2008, pp. 4688–4692.

[161] Schaart D. R., van Dam H. T., Seifert S., Vinke R., Dendooven p., Löhner H. and Beekman F. J., *Phys. Med. Biol.*, **54** (2009) 3501.

[162] van Dam H. T., Seifert S., Vinke R., Dendooven P., Löhner H., Beekman F. J. and Schaart D. R., *Phys. Med. Biol.*, **56** (2011) 4135.

[163] van Dam H T., Borghi G., Seifert S. and Schaart D., *Phys. Med. Biol.*, **58** (2013) 3243.

[164] González Antonio J., Majewski Stan, Proffitt James, Aguilar Albert, Conde Pablo, Hernandez Liczandro, Sánchez Filomeno, Stolin Alexander and Benlloch Jose M., *Continuous or pixelated scintillators?, not longer a discussion,* in *IEEE NSS-MIC Conference Record*, (IEEE) 2014.

[165] Conde P., González A. J., Hernández L., Bellido P., Iborra A., Crespo E., Moliner L., Rigla J. P., Rodríguez-Álvarez M. J., Sánchez F., Seimetz M., Soriano A., Vidal L. F. and Benlloch J. M., *Nucl. Instrum. Methods A*, **734-B** (2014) 132.

[166] Peet B. J., Borghi G., Tabacchini V. and Schaart D., *J. Nucl. Med.*, **56** (2015) 602.

[167] Pani R., Gonzalez A. J., Bettiol M., Fabbri A., Cinti M. N., Preziosi E., Borrazzo C., Conde P., Pellegrini R., Di Castro E. and Majewski S., *J. Instrum.*, **10** (2015) C06006.

[168] González A. J., Conde P., Iborra A., Aguilar A., Bellido P., García-Olcina R., Hernández L., Moliner L., Rigla J. P., Rodríguez-Álvarez M. J., Sánchez F., Seimetz M., Soriano A., Torres J., Vidal L. F. and Benlloch J. M., *Nucl. Instrum. Methods A*, **787** (2015) 42.

[169] Gonzalez A. J. *et al.*, *IEEE Trans. Nucl. Sci.*, **63** (2016) 2471.

[170] Borghi G., Peet B. J., Tabacchini V. and Schaart D. R., *Phys. Med. Biol.*, **61** (2016) 4929.

[171] Morrocchi M., Hunter W. C. J., Del Guerra A., Lewellen T. K., Kinahan P. E., MacDonald L. R., Bisogni M. G. and Miyaoka R. S., *Med. Biol.*, **61** (2016) 8298.

[172] González A., Aguilar A., Conde P., Hernández L., Moliner L., Vidal L. F., Sánchez F., Sánchez S., Correcher C., Molinos C., Barbera J., Lankes K., Junge S., Bruckbauer T., Bruyndonckx P. and Benlloch J. M., *IEEE Trans. Nucl. Sci.*, **63** (2016) 2471.

[173] Morrocchi Matteo, Ambrosi Giovanni, Bisogni Maria Giuseppina, Bosi Filippo, Boretto Marco, Cerello Piergiorgio, Ionica Maria, Liu Ben, Pennazio Francesco, Piliero Maria Antonietta, Pirrone Giovanni, Postolache Vasile, Wheadon Richard and Del Guerra Alberto, *EJNMMI Phys.*, **4** (2017) 11.

[174] González-Montoro Andrea, Sánchez Filomeno, Martí Rosana, Hernández Liczandro, Aguilar Albert, Barberá Julio, Catret Juan V., Cañizares Gabriel, Conde Pablo, Lamprou Efthymios, Martos Francisco, Sánchez Sebatián, Vidal Luis F. and Benlloch Jose M., *Nucl. Instrum. Methods Phys. Res. A*, **912** (2018) 372.

[175] Muller Florian, Schug David, Hallen Patrick, Grahe Jan and Schulz Volkmar, *IEEE Trans. Radiat. Plasma Med. Sci.*, **3** (2019) 465.

[176] Pierce L. A., Pedemonte S., DeWitt D., MacDonald L., Hunter W. C. J., Van Leemput K. and Miyaoka R., *Phys. Med. Biol.*, **63** (2018) 075017.

[177] Panetta J. V., Surti S., Singh B. and Karp J. S., *IEEE Trans. Radiat. Plasma Med. Sci.*, **3** (2019) 531.

[178] Gonzalez-Montoro A. *et al.*, *Nucl. Instrum. Methods Phys. Res. A*, **920** (2019) 58.

[179] Stockhoff M., Van Holen R. and Vandenberghe S., *Phys. Med. Biol.*, **64** (2019) 195003.

[180] Belcari Nicola, *UTOFPET: design of a highly scalable TOF-PET detector concept*, presented at the FATA 2019, 3–5 September 2019, Acireale (Italy), `https://agenda.infn.it/event/18991/timetable/`.

[181] Surti S., *J. Nucl. Med.*, **56** (2015) 98.

[182] Surti S. and Karp J. S., *Phys. Med.*, **32** (2016) 12.

[183] Cates J. W. and Levin C. S., *Phys. Med. Biol.*, **61** (2016) 2255.

[184] Vandenberghe S., Mikhaylova E., D'Hoe E., Mollet P. and Karp J. S., *EJNMMI Phys.*, **3** (2016) 3.

[185] Prior John, *The 10-ps TOF PET: Clinical applications,* presented at the FATA 2019, 3–5 September 2019, Accademia degli Zelanti e dei Dafnici, Acireale (Catania, Italy), https://agenda.infn.it/event/18991/timetable/.
[186] Conti Maurizio, *Siemens Biograph Vision and the future of TOF-PET*, presented at the FATA 2019, 3–5 September 2019, Acireale (Italy), https://agenda.infn.it/event/18991/timetable/.
[187] Nuyts Johan, *Using time-of-flight information for PET reconstruction in PET, PET/CT and PET/MRI*, presented at the FATA 2019, 3–5 September 2019, Acireale (Italy), https://agenda.infn.it/event/18991/timetable/.
[188] Rezaei A., Defrise M., Bal G., Michel C., Conti M., Watson C. and Nuyts J., *IEEE Trans. Med. Imaging*, **31** (2012) 2224.
[189] Defrise M., Rezaei A. and Nuyts J., *Phys. Med. Biol.*, **57** (2012) 885.
[190] Conti M., Hong I. and Michel C., *Phys. Med. Biol.*, **57** (2012) 307.
[191] Defrise M., Rezaei A. and Nuyts J., *Phys. Med. Biol.*, **59** (2014) 1073.
[192] Rezaei A., Defrise M. and Nuyts J., *IEEE Trans. Med. Imaging*, **33** (2014) 1563.
[193] Salvo K. and Defrise M., *Phys. Med. Biol.*, **62** (2017) 8283.
[194] Rezaei A., Deroose C. M., Vahle T., Boada F. and Nuyts J., *J. Nucl. Med.*, **59** (2018) 1630.
[195] Hwang D., Kang S. K., Kim K. Y., Seo S., Paeng J. C., Lee D. S. and Lee J. S., *J. Nucl. Med.*, **60** (2019) 1183.
[196] Grant A. M., Deller T. W., Khalighi M. M., Maramraju S. H., Delso G. and Levin C. S., *Med. Phys.*, **43** (2016) 2334.
[197] Yang Y., St James S., Wu Y. B. *et al.*, *Phys. Med. Biol.*, **56** (2011) 139.
[198] Vilardi I. *et al.*, *Nucl. Instrum. Methods Phys. Res. A*, **564** (2006) 506.
[199] Levin C., *IEEE Trans. Nucl. Sci.*, **49** (2002) 2236.
[200] Yeom J. Y., Vinke R., Bieniosekl M. F. and Levin C. S., *Comparison of end/side scintillator read-out with digital-SiPM for TOF PET,* in *IEEE MIC Conference Record*, M21–38 (IEEE) 2013, https://doi.org/10.1109/NSS-MIC.2013.6829322.
[201] Gundacker S., Knapitsch A., Auffray E., Jarron P., Meyer T. and Lecoq P., *Nucl. Instrum. Methods Phys. Res. Sect. A*, **737** (2014) 92.
[202] Seifert S. and Schaart D. R., *IEEE Trans. Nucl. Sci.*, **62** (2015) 3.
[203] Derenzo S. E., Choong W.-S. and Moses W. W., *Phys. Med. Biol.*, **60** (2015) 7309.
[204] Han Young Been, Kang Han Gyu, Song Seong Hyun, Kim Kyeong Min, Ko Guen Bae, Lee Jae Sung and Hong Seong Jong, *A study on the SiPM based dual-ended readout TOF-PET PET module*, presented at the IEEE MIC, Atlanta, 21–28 October 2017.
[205] Derenzo Stephen E., *Phys. Med. Biol.*, **62** (2017) 3828.
[206] Zhang X., Peng Q., Zhou J., Huber J. S., Moses W. W. and Qi J., *Phys. Med. Biol.*, **63** (2018) 065010.
[207] Du J., Yang Y., Bai X., Judenhofer M. S., Berg E., Di K., Buckley S., Jackson C. and Cherry S. R., *IEEE Trans. Nucl. Sci.*, **63** (2016) 8.
[208] Spanoudaki V. C. and Levin C. S., *Sensors.*, **10** (2010) 10484.
[209] Roncali E. and Cherry S. R., *Ann. Biomed. Eng.*, **39** (2011) 1358.
[210] Yamazaki M., Takeshita T. and Hasegawa Y., *J. Instrum.*, **8** (2013) P02018.
[211] Piatek S., *Physics and Operation of the MPPC Silicon Photomultiplier* (Prentice Hall) 2014.
[212] Matsuda H., Kataoka J., Ikeda H., Kato T., Anbe T., Nakamura S., Ishikawa Y., Sato K. and Yamamura K., *Nucl. Instrum. Methods Phys. Res. Sect. A*, **699** (2013) 211.
[213] MPPC TOF module for PET (C13500-4075LC-12), Technical Note, Hamamatsu, www.hamamatsu.com, Cat. No. KACC9009E03, Jan. 2017.
[214] Gonzalez A. J., Conde P., Hernández L., Sanchez F., Aguilar A., Majewski S., Garcia-Olcina R., Torres J. and Benlloch J. M., *Position sensitive photosensors based on SiPM arrays,* in *IEEE Sensors Conference Record (Valencia, Spain)* (IEEE) 2014.

[215] Ferri A., Gola A., Serra N., Tarolli A., Zorzi N. and Piemonte C., *Phys. Med. Biol.*, **59** (2014) 869.
[216] Auffray E. *et al.*, *J. Instrum.*, **10** (2015) P06009.
[217] Hsu D. F., Ilan E., Peterson W. T., Uribe J., Lubberink M. and Levin C. S., *J. Nucl. Med.*, **58** (2017) 1511.
[218] Spanoudaki V. Ch. and Levin C. S., *Phys. Med. Biol.*, **56** (2011) 735.
[219] Nemallapudi M. V., Gundacker S., Lecoq P., Auffray E., Ferri A., Gola A. and Piemonte C., *Phys. Med. Biol.*, **60** (2015) 4635.
[220] Gundacker S., Acerbi F., Auffray E., Ferri A., Gola A., Nemallapudi M., Paternoster G., Piemonte C. and Lecoq P., *J. Instrum.*, **11** (2016) P08008.
[221] Schotanus Paul, *Fast timing with scintillation detectors*, presented at the FATA 2019, 3–5 September 2019, Acireale (Italy), `https://agenda.infn.it/event/18991/timetable/`.
[222] Mirabelli Riccardo, *TOPS Project: Development of new fast timing plastic scintillators*, presented at the FATA 2019, 3–5 September 2019, Acireale (Italy), `https://agenda.infn.it/event/18991/timetable/`.
[223] Kim H., Chen C. T., Chen H. T., Ronzhin A., Ramberg E., Los S., Murat P., Majewski S. and Kao C. M., *A TOF PET detector development using waveform sampling and strip-line based data acquisition,* in *IEEE MIC Conference Record*, M16–56 (IEEE) 2013.
[224] Ronzhin A., Albrow M., Los S., Martens M., Murat P., Ramberg E., Kim H., Chen C., Kao C. and Niessen K., *Nucl. Instrum. Methods Phys. Res. Sect. A*, **703** (2013) 109.
[225] Torres J., Aguilar A., García-Olcina R., Martos J., Soret J., Benlloch J. María, González A. J. and Sánchez F., *Nucl. Instrum. Methods Phys. Res. Sect. A*, **702** (2013) 73.
[226] Bugalho R., Rolo M. D., Zorraquino C., Silva R., Silva J. C., Veckalns V., Wheadon R., Rivetti A., Tavernier S. and Varela J., *Design and performance of an ASIC for TOF applications,* in *IEEE MIC Conference Record*, NPO2–221 (IEEE) 2013.
[227] Aguilar A., González A. J., Torres J., García-Olcina R., Martos J., Soret J., Conde P., Hernández L., Sánchez F. and Benlloch J. M., *Trans. Nucl. Sci.*, **62** (2014) 12.
[228] Casella C., Heller M., Joram C. and Schneider T., *Nucl. Instrum. Methods Phys. Res. Sect. A*, **736** (2014) 161.
[229] Gundacker S., Auffray E., Jarron P., Meyer T. and Lecoq P., *Nucl. Instrum. Methods Phys. Res. Sect. A*, **787** (2015) 6.
[230] Francesco D., Bugalho R., Oliveira L., Pacher L., Rivetti A., Rolo M., Silva J., Silva R. and Varela J., *J. Instrum.*, **11** (2016) C03042.
[231] González A. J., Majewski S., Barberá J., Conde P., Correcher C., Hernández L., Morera C., Vidal San Sebastian L. F., Sánchez F., Stolin A. and Benlloch J. M., *Trans. Nucl. Sci.*, **62** (2014) 19.
[232] Gundacker S., Auffray E., Frisch B., Jarron P., Knapitsch A., Meyer T., Pizzichemi M. and Lecoq P., *J. Instrum.*, **8** (2013) P07014.
[233] Lecoq P., *IEEE Trans. Radiat. Plasma Med. Sci.*, **1** (2017) 473.
[234] Borghi Giacomo and Gola Alberto, *Photodetectors for fast timing*, presented at the FATA 2019, 3–5 September 2019, Acireale (Italy), `https://agenda.infn.it/event/18991/timetable/`.
[235] Ahmad Salleh, *Recent developments in fast timing ASICs for particle physics and medical imaging*, presented at the FATA 2019, 3–5 September 2019, Acireale (Italy), `https://agenda.infn.it/event/18991/timetable/`.
[236] Lecoq Paul, *Ultrafast meta-scintillators for a new generation of HEP detectors and Time-of-Flight PET*, presented at the FATA 2019, 3–5 September 2019, Acireale (Italy), `https://agenda.infn.it/event/18991/timetable/`.

[237] Tavernier Stefaan, *Electronics for fast timing in medical imaging*, presented at the FATA 2019, 3–5 September 2019, Acireale (Italy), https://agenda.infn.it/event/18991/timetable/.
[238] Pestotnik Rok, *Using Cherenkov light in TOF-PET*, presented at the FATA 2019, 3–5 September 2019, Acireale (Italy), https://agenda.infn.it/event/18991/timetable/.
[239] Venturini Yuri, *New approaches to detector readout in particle physics and medical applications with efficient timing*, presented at the FATA 2019, 3–5 September 2019, Acireale (Italy), https://agenda.infn.it/event/18991/timetable/.
[240] González Antonio J., Sánchez Filomeno, Majewski Stan, Aguilar Albert, González-Montoro Andrea, Parkhurst Philip, Vaigneur Keith and Benlloch José M., *Performance of large BGO arrays coupled to SiPM photosensors – continued study,* in *2015 IEEE Nuclear Science Symposium and Medical Imaging Conference (NSS/MIC)* (IEEE) 2015, https://doi.org/10.1109/NSSMIC.2015.7582017.
[241] González Antonio J., Sánchez Filomeno, Majewski Stan, Parkhurst Philip, Vaigneur Keith and Benlloch José M., *IEEE Trans. Nucl. Sci.*, **63** (2016) 2482.
[242] Gonzalez-Montoro Andrea, Sanchez Filomeno, Majewski Stan, Zanettini Silvia, Benlloch Jose M. and Gonzalez Antonio J., *J. Instrum.*, **12** (2017) C11027.
[243] Gundacker Stefan, Turtos Rosana Martinez, Auffray Etiennette, Paganoni Marco and Lecoq Paul, *Phys. Med. Biol.*, **64** (2019) 055012.
[244] Kwon S. I., Roncali E., Gola A., Paternoster G., Piemonte C. and Cherry S. R., *Phys. Med. Biol.*, **64** (2019) 105007.
[245] Cates Joshua W. and Levin Crai S., *Phys. Med.*, **64** (2019) 175016.
[246] Minot Michael, *Large Area Picosecond Photodetector (LAPPD) offers fast timing for HEP, NP and medical imaging*, presented at the FATA 2019, 3–5 September 2019, Acireale (Italy), https://agenda.infn.it/event/18991/timetable/.
[247] Jiang Jianyong, Samanta Suranjana, Li Ke, Siegel Stefan B., Mintzer Robert A., Cho Sanghee, Conti Maurizio, Schmand Matthias, O'Sullivan Joseph, Tai Yuan-Chuan, *Augmented whole-body scanning via magnifying PET*, *IEEE Trans. Med. Imaging*, https://doi.org/10.1109/TMI.2019.2962623.
[248] Soret M., Bacharach S. L. and Buvat I., *J. Nucl. Med.*, **48** (2007) 932.
[249] Guillette N., Sarrhini O., Lecomte R. and Bentourkia M., *Correction of partial volume effect in the projections in PET studies,* in *IEEE Nuclear Science Symposium & Medical Imaging Conference, Knoxville, TN* (IEEE) 2010, pp. 3541–3543.
[250] Erlandsson K., Buvat I., Pretorius P. H., Thomas B. A. and Hutton B. F., *Phys. Med. Biol.*, **57** (2012) R119.
[251] Cysouw M. C. F., Golla S. V. S., Frings V. *et al.*, *EJNMMI Res.*, **9** (2019) 12.
[252] Yang J., Hu C., Guo N. *et al.*, *Sci. Rep.*, **7** (2017) 13035.
[253] Boto E., Holmes N., Leggett J., Roberts G., Shah V., Meyer S. S., Munoz L. D., Mullinger K. J., Tierney T. M., Bestmann S., Barnes G. R., Bowtell R. and Brookes M. J., *Nature*, **555** (2018) 657.